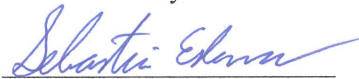


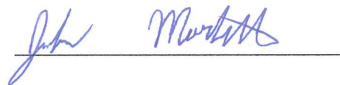
Design of a Micro-Pulsed Plasma Thruster for a 3U Cubesat

A Major Qualifying Project Report
Submitted to the Faculty of the
WORCESTER POLYTECHNIC INSTITUTE
in Partial Fulfillment of the Requirements for the
Degree of Bachelor of Science
In Aerospace Engineering

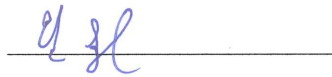
by



Sebastian A. Eslava



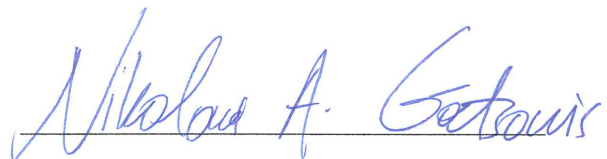
Jordan D. Marchetto



Erik A. Scougal

March 17, 2014

Approved by:



Professor Nikolaos A. Gatsonis, Advisor
Aerospace Engineering Program
Mechanical Engineering Department, WPI

Abstract

This project presents the conceptual design of a micro-Pulsed Plasma Thruster (microPPT) and a propulsion module consisting of eight micro-PPTs for applications on a three-unit Cube Satellite (3U CubeSat). The computer aided mechanical design of the micro-PPT, the propulsion module and its integration in the 1U are presented. Material selection identifies Torlon 4203 for housing and Tungsten-plated copper for electrodes. Finite element stress analysis shows that the micro-PPT will sustain expected launch loads. The electric circuit for the main and initial discharge are designed and simulated for power and voltage levels expected in a 3U Cubesat. Finite element thermal analysis provides estimates of the temperature distribution in the micro-PPT and module for a typical discharge.

“Certain materials are included under the fair use exemption of the U.S. Copyright Law and have been prepared according to the fair use guidelines and are restricted from further use.”

Acknowledgements

We would like to thank the following individuals and groups for their help and support throughout the entirety of this project.

Project Advisor Professor Nikolaos Gatsonis

Computational Support Professor Adriana Hera

Table of Authorship

Section	Author
<i>1 Introduction</i>	1.0, 1.1, 1.2, and 1.3.2 Sebastian Eslava 1.3.1 Jordan Marchetto 1.3.3 Erik Scougal
<i>2.0 Mechanical and Structural Design</i>	Jordan Marchetto 2.2 Electrode Erik Scougal
<i>3.0 Electrical Design</i>	<i>Sebastian Eslava</i>
<i>4.0 Thermal Modeling</i>	Erik Scougal
<i>5.0 Conclusions</i>	5.0, 5.1.2 Sebastian Eslava 5.1.1 Jordan Marchetto 5.1.3 Erik Scougal

Table of Contents

Acknowledgements.....	2
Table of Authorship	3
Table of Contents	4
Table of Figures	6
Table of Tables	9
Chapter 1 Introduction	10
1.1 Review of Cubesats.....	10
1.2 Review of PPTs.....	12
1.3 Design Objectives, Requirements, Approach and Methods.....	15
1.3.1 Mechanical Design and Structural Analysis	17
1.3.2 Electrical Design and Analysis.....	17
1.3.3 Thermal Design and Analysis.....	18
Chapter 2: Mechanical Design.....	19
2.1 Mechanical Design and Requirements.....	19
2.2 Material Selection	20
2.3 Design Iterations	24
2.4 ANSYS Structural Analysis	32
2.5 Cubesat Integration	35
Chapter 3 Electrical Design and Analysis	36
3.1 Vacuum Arc Ignition System.....	36
3.2 Integration of Vacuum Arc Ignition Circuit with Power Management and Distribution System.....	38
3.3 Vacuum Arc Ignition Circuit.....	44
Chapter 4 Thermal Design and Analysis	52
4.1 Validation of Finite Element Analysis	52
4.2 Pulsed Thermal Analysis.....	56
4.3 Pulsed Model Validation.....	63
4.4 Thermal Performance of the micro-PPT Design.....	69

5.0 Conclusions and Recommendations	78
5.1 Conclusions	78
5.1.1 Mechanical Design and Structural Analysis.....	78
5.1.2 Electrical Design and Analysis.....	80
5.1.3 Thermal Design and Analysis Model.....	81
5.2 Recommendations for Future Work.....	81
Bibliography	83

Table of Figures

Figure 1: Cal Poly 1U and 3U Cubesate design specifications in mm (Munakata 2009).	11
Figure 2: 3U Specifications in mm (Munakata et al., 2009).....	11
Figure 3: Magentic field (white arrows) and forces (black arrows) from COMSOL simulation of a PPT.....	13
Figure 4: Flanged plate PPT configuration (Marques et al., 2009)	13
Figure 5: Parallel plate PPT configuration.....	14
Figure 6: PPT with circuit model (Laperriere et al., 2005).....	14
Figure 7: SolidWorks model of inital parallel plate micro-PPT design.....	19
Figure 8: Results of second stage CES selection. Copyright 2013 Granta.....	22
Figure 9: Results of third stage CES selection. Copyright 2013 Granta	22
Figure 10: Flat notched electrode plate.....	25
Figure 11: Electrode design with L-shaped cross section.....	25
Figure 12: Teflon and Electrode-Casing Assembly Held Together by Spring Compression.	26
Figure 13: Initial Case-Spring Design.	27
Figure 14: Completed Structural Design.	27
Figure 15: Internal View of Completed Structure.	28
Figure 16: PPT Performance Model GUI (Laperriere et al, 2005).....	29
Figure 17: Alternate PPT design casing.....	30
Figure 18: Front (left) and back (right) views of Alternate PPT casing.	30
Figure 19: Isometric view of Finalized design.	31
Figure 20: Final design with transparent casing to show internal portion.....	31
Figure 21: General Environmental Verification Standard for random vibration.....	32
Figure 22: Von Mises Stresses from ANSYS simulation.....	33
Figure 23: X-directional Deformation.	33
Figure 24: Y-Directional deformation.	34
Figure 25: Z-directional deformation.....	34
Figure 26: PPT's mounted on 1U of Cubesat.....	35

Figure 27: Clyde-Space's 3U CubeSat EPS (Strain 2010).....	38
Figure 28: Clyde-Sapce's 3U CubeSat EPS (Strain 2010).....	39
Figure 29: CubeSat Header Pins (Strain 2010).....	40
Figure 30: Signals controlling vacuum arc ignition circuit of the micro-PPT.....	43
Figure 31: Initial Discharge Circuit	44
Figure 32: EMCO G25 proportional booster (EMCO).....	44
Figure 33: EMCO G25 Output voltage characteristics (EMCO).....	45
Figure 34: Input pulse signal.....	46
Figure 35: PSPICE circuit for simulation purposes charging configuration.	46
Figure 36: PSPICE circuit for simulation purposes discharging configuration.....	47
Figure 37: PSPICE marx circuit results	47
Figure 38: Calramic capacitor specifications (calramic, 2013)	48
Figure 39: PCB board layout for initial discharge.....	49
Figure 40: Rimfire spark plug (Rimfire).....	49
Figure 41: Main discharge circuit of the micro-PPT.	50
Figure 42: Main discharge initial design.	51
Figure 43: Main discharge PCB board layout.....	51
Figure 45: Analytical solution to Case 1.....	53
Figure 46: ANSYS solution to Case 1.	53
Figure 47: COMSOL solution to Case 1.....	54
Figure 48: Temperature profile in Teflon of XPPT-1. (Stechmann, 2007)	55
Figure 49: ANSYS solution to Case 2.	55
Figure 50: COMSOL solution to Case 2.....	56
Figure 51: Time varying heat flux profile. (Stechmann, 2007)	57
Figure 52: Teflon face pulse response from COMSOL.....	58
Figure 53: Pulse response with cooling from COMSOL.....	58
Figure 54: 2-D long pulse error in ANSYS.	59
Figure 55: 2-D long pulse error in COMSOL.....	59
Figure 56: Rectangular pulse input function.....	61
Figure 57: Up-close pulse modulation function.....	61
Figure 58: 1 period modulation function	62

Figure 59: Elongated pulse length.	62
Figure 60: Up-close pulse of heat flux function.	63
Figure 61: Pulsed thermal model COMSOL simulation of Case 2.	64
Figure 62: COMSOL simulation of Case 2 at 10sec +1 pulse.....	64
Figure 63: Simulation for Case 2 at 11sec.....	65
Figure 64: Micro-PPT Geometry in COMSOL.	66
Figure 65: Micro-PPT meshed in COMSOL.....	67
Figure 66: Average value of Teflon face temperature for high thermal flux.....	68
Figure 67: Average value of electrode face temperature for high thermal flux.....	68
Figure 68: Average value of casing face temperature for high thermal flux.	68
Figure 69: Teflon domain average face temperature with high thermal flux.	69
Figure 70: Temperature distribution in a micro-PPT after a pulse.	71
Figure 71: Temperature distribution micro-PPT after a train.	71
Figure 72: Average Teflon face temperature in the micro-PPT.	72
Figure 73: Average electrode face temperature in the micro-PPT.	72
Figure 74: Average casing face temperature in the micro-PPT.....	72
Figure 75: Maximum electrode temperature in the micro-PPT.....	73
Figure 76: Maximum casing temperature in the micro-PPT.	73
Figure 77: Pulse maximum electrode temperature, firing 1-10.....	74
Figure 78: Pulse maximum electrode temperature, firing 11-21.....	74
Figure 79: Pulse maximum casing temperature, firing 1-8.....	75
Figure 80: Pulse maximum casing temperature, firing 11-21.....	75
Figure 81: Final Model.	79
Figure 82: 3-axis control configuration	80

Table of Tables

Table 1: Cubesat Flights with size, activity, and launch date.....	12
Table 2: Flight Proven PPT's and characteristics.....	15
Table 3 Typical Performance and Ablation Parameters of the micro-PPT.	16
Table 4: Values for initial CES selection stage	22
Table 5: Erosion characteristics of electrode materials (Shaw, 2011).....	23
Table 6: Torlon 4203 Data Sheet.....	24
Table 7: Methods for Vacuum Arc Ignition.	37
Table 8: PMD Connection Capabilities.....	41
Table 9: Switch Number, Voltage level and current ratings.....	41
Table 10: Header Pin Designations.....	42
Table 11: EMCO proportional booster specifications.	45
Table 12: Input parameters for Case 1 validation.....	52
Table 13: XPPT-1 characteristics.	54
Table 14: Discretization of the transient heat flux profile.....	57
Table 15: Parameters of sample rectangular thermal input function to COMSOL.	60
Table 16: Material used in COMSOL thermal analysis of micro-PPT.....	66
Table 17: Parameters of full micro-PPT thermal simulation in COMSOL.....	67
Table 18: Parameters used in thermal analysis of the micro-PPT.	70
Table 19: Temperature Slope values.....	76
Table 20: Worst Case Approximation Electrode and Casing Temperatures at 20000s....	76
Table 21: Melting points of micro-PPT materials.....	77

Chapter 1 Introduction

Pulsed Plasma Thrusters (PPTs) have been considered for a variety of missions (Gatsonis et al.) and can become an attractive option for a Cubesat's propulsion subsystem due to their low power input, high specific impulse, and ease of geometric scalability (Gatsonis et al 2001, Partridge 2008). They achieve thrust without moving parts by accelerating high velocity ions and slow neutral gas particles with electromagnetic pressure and aerodynamic pressure gradients. PPTs are currently limited by their low efficiency, typically around 10%. In this Major Qualifying Project (MQP) we attempt to initiate the development of a more efficient Teflon-fed parallel plate Micro-PPT for integration with a 3U Cubesat. WPI's Aerospace Engineering Department has conducted studies on how to develop a Cubesat mission for a 3U satellite (Billings et al. 2013). This MQP addresses how to design the Micro-PPT from an electrical, structural, and thermal standpoint in order to meet the propulsion subsystem requirements of a 3U Cubesat.

1.1 Review of Cubesats

Cubesats are a class of nano-satellites that follow Cubesat Design Specifications (CDS) published by California Polytechnic State University (Cal Poly). Cubesats are aimed to streamline the spacecraft design process in a cost effective manner. An organization can build a Cubesat at low development costs because commercially-off-the-shelf (COTS) components typically make up the design. Cubesats are an attractive option for universities that wish to access space for research purposes.

Cubesats typically take up a 1 liter volume, measuring $10 \times 10 \times 10 \text{ cm}^3$, and weigh 1kg. Cubesats that adhere to the 1 liter and 1kg sizing constraint are commonly called "1U" as in "1 Unit" for short. Cubesat sizes are scalable to 2U ($1 \times 1 \times 2 \text{ cm}^3$), 3U ($1 \times 1 \times 3 \text{ cm}^3$), and larger variations. Figure 1 and 2 illustrate Cal Poly's CDS for 1U and 3U Cubesats (Munakata, 2009).

The Cubesat concept drifts away from the custom-built spacecraft culture. The standardization of Cubesat size and weight allows for an increase in ride share opportunities. The Poly Pico-satellite Orbital Deployer (P-POD), developed by Stanford University and Cal Poly, is a common deployment system for Cubesats of various sizes (Munakata 2009). The P-POD has

been used to deploy 75% of all Cubesats launched (Crook 2009). P-POD simplicity allows for easy integration between launch vehicles and secondary payloads such as Cubesats.

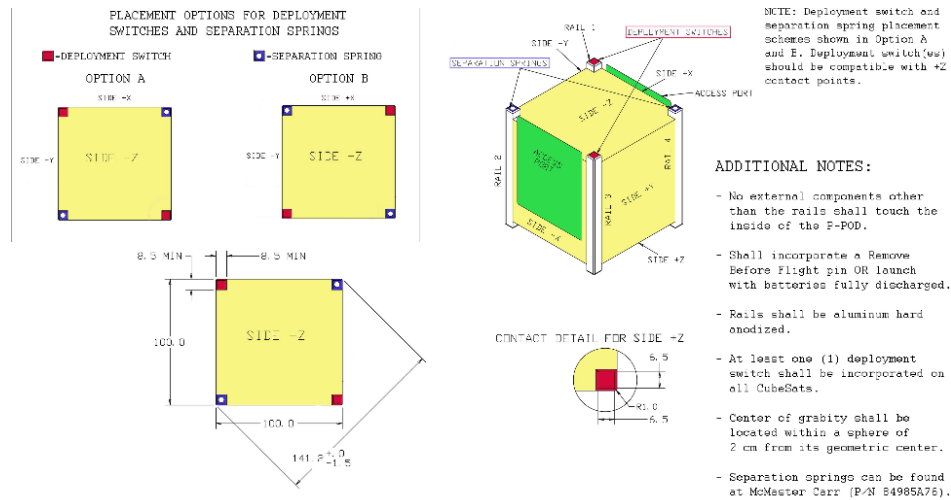


Figure 1: Cal Poly 1U and 3U Cubesat design specifications in mm (Munakata 2009).

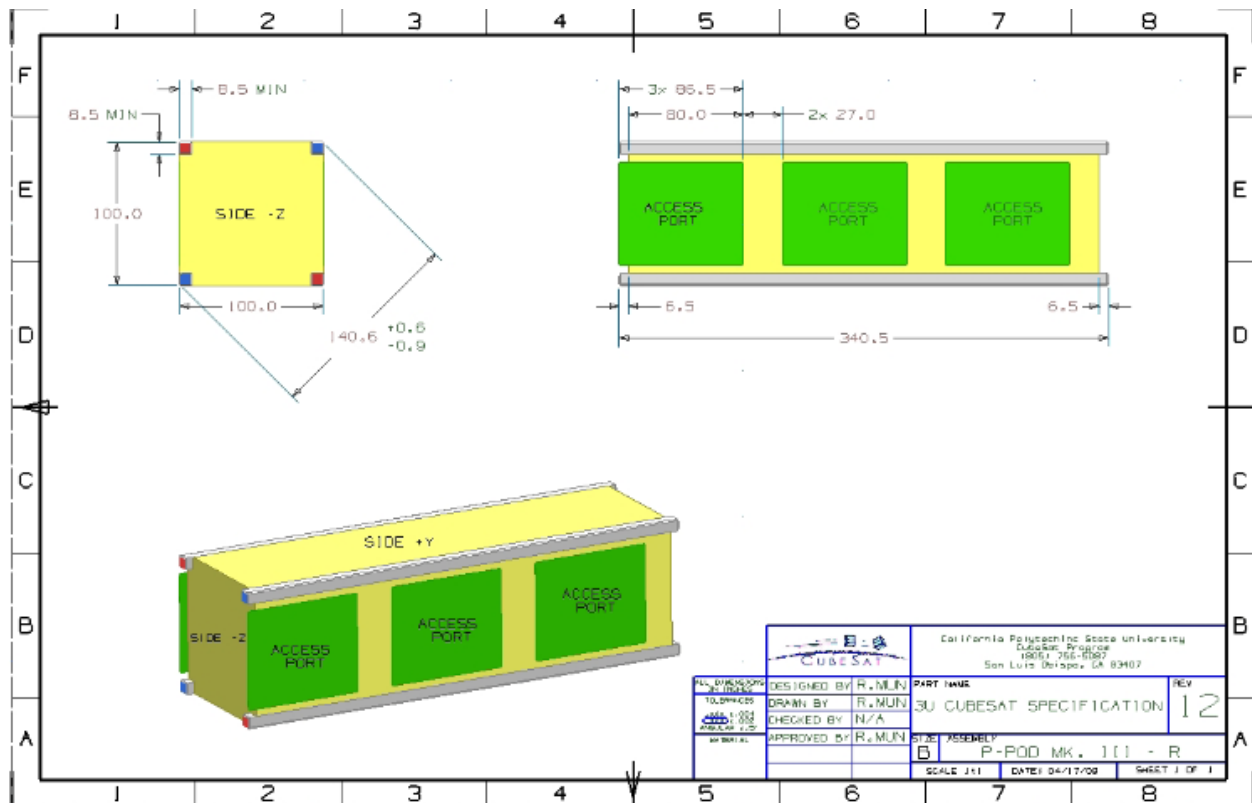


Figure 2: 3U Specifications in mm (Munakata et al., 2009)

Space science and exploration have benefited from the streamlined approach because less time is invested towards the space mission analysis phase. Cubesats were introduced in 1999 and since then many have flown as seen in Table 1.

Table 1: Cubesat Flights with size, activity, and launch date.

Launch Date	Name	Contractor/University	Size	Activity	Propulsion
2/10/2000	PICOSAT 3 (JAK)	Santa Clara University	Opal	not active	none
2/10/2000	PICOSAT 6 (StenSat)	Stensat Group, LLC	Opal	not active	none
2/12/2000	PICOSAT 4 (Thelma)	Santa Clara University	Opal	not active	none
2/12/2000	PICOSAT 5 (Louise)	Santa Clara University	Opal	not active	none
9/6/2001	PICOSAT 7&8 (TETHERED)	Aerospace Corp	Opal	diactivated	none
12/2/2002	MEPSI	Aerospace Corporation. NASA Jet Propulsion Laboratory	2U	diactivated	none
6/30/2003	DTUSAT 1	Technical University of Denmark	1U	not active	none
6/30/2003	CUTE-1 (CO-55)	Tokyo Institute of Technology	1U	not active	none
6/30/2003	QUAKESAT 1	Stanford University	3U	not active	none
6/30/2003	AAU CUBESAT 1	University of Aalborg	1U	not active	none
6/30/2003	CANX-1	UTIAS (University of Toronto)	1U	not active	none
6/30/2003	CUBESAT XI-IV (CO-57)	University of Tokyo	1U	semi-operation	none
10/27/2005	UWE-1	University of Würzburg	1U	not active	none
10/27/2005	CUBESAT XI-V (CO-58)	University of Tokyo	1U	not active	none
10/27/2005	Ncube 2	Norwegian Universities	1U	not active	none
2/21/2006	CUTE 1.7	Tokyo Institute of Technology	2U	diactivated	none
7/26/2006	CP 1 (K7RR-Sat)	Cal Poly San Luis Obispo	1U	diactivated	none
7/26/2006	CP 2	Cal Poly San Luis Obispo	1U	diactivated	none
7/26/2006	HAUSAT 1	Hankuk Aviation University	1U	diactivated	none
7/26/2006	ICECube 1	Cornell University	1U	diactivated	none
7/26/2006	ICECube 2	Cornell University	1U	diactivated	none
7/26/2006	ION	University of Illinois	2U	diactivated	none
7/26/2006	KUTESat Pathfinder	University of Kansas	1U	diactivated	none
7/26/2006	Mea Huaka'i (Voyager)	University of Hawaii	1U	diactivated	none
4/28/2008	DELFI C3 (DO-64)	Technical University of Delft	3U	active	none
4/28/2008	CANX 2	UTIAS (University of Toronto)	3U	active	none
4/28/2008	SEEDS 2 (CO-66)	Nihon University	1U	active	none
8/3/2008	PreSat	NASA Ames Research Center	3U	active	none
8/3/2008	NanoSail D	NASA Ames Research Center	3U	active	none
11/15/2008	PSSC-Testbed 1	Aerospace Corp	2U	active	none
12/1/2013	Aero-Cube 5a	Aerospace Corporation	1U	diactivated	none
12/1/2013	Aero-Cube 5b	Aerospace Corporation	1U	diactivated	none
12/1/2013	ALICE	Air Force Institute of Technology	3U	diactivated	none
12/1/2013	CUNYSat-1	City University of New York	1U	diactivated	none
12/9/2013	KickSat	Cornell University	3U	diactivated	none
12/9/2013	PhoneSat (v2.5)	NASA Ames	1U	diactivated	none
12/9/2013	TSAT	Taylor University	2U	diactivated	none
12/9/2013	ALL-STAR/THEIA	University of Colorado	3U	diactivated	none
12/9/2013	SporeSat	NASA Ames	3U	diactivated	none
12/29/2013	ArduSat 1	NanoSatisfi	1U	diactivated	none
12/29/2013	ArduSat X	NanoSatisfi	1U	diactivated	none
12/29/2013	PicoDragon	Vietnam National Satellite Center	1U	diactivated	none

Table 1 indicates that all Cubesats developed do not have propulsion systems and the majority of them are inactive. A propulsion system on board a Cubesat could solve the issue of inactivity. A propulsion subsystem could be used to detumble a Cubesat with 3 axis control. The micro-PPT we designed in this MQP provides more compact control than the current bulky methods used with magneto-torquers.

1.2 Review of PPTs

Pulsed Plasma Thrusters are the first Electric Propulsion (EP) technology to ever fly in space. PPTs are an attractive technology for their high specific impulse, I_{sp} , and low mass characteristics. PPTs have been explored extensively at WPI including performance and plume measurements (Gatsonis et al. 2001; Gatsonis et al, 2004; Laperrriere et al, 2005), ablation

modeling (Gatsonis et al, 2007; Stechmann, 2007), as well as micro-PPTs with water propellant (Partridge and Gatsonis; 2005; Partidge, 2008).

PPTs generate thrust by transferring energy stored in a capacitor to an electromagnetic field that accelerates plasma through a Lorentz Force ($J \times B$ Force). The electromagnetic field is generated with two electrode plates that conduct the capacitor's current. The electric field lines form inside the electrode plates. The magnetic field wraps around the current and penetrates the electric field between the plates. Figure 3 illustrates the variation in intensity of the electric field between the plates from a COMSOL simulation assuming magnetostatics. The direction of the magnetic field curling around the parallel plates is also shown with white arrows.

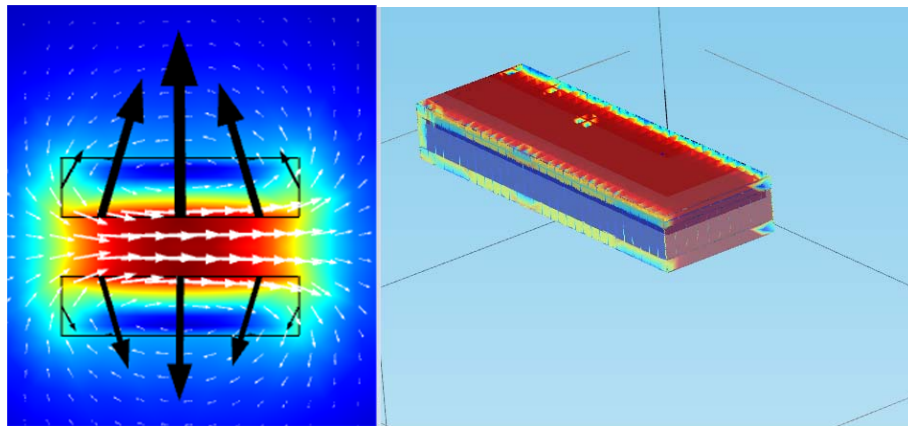


Figure 3: Magnetic field (white arrows) and forces (black arrows) from COMSOL simulation of a PPT.

The PPT geometry shown in Figure 3 is that of a typical parallel plate configuration. Figure 4 illustrates a flanged plate configuration (Marques et al, 2009) and Figure 5 shows a parallel plate configuration used in this design study.

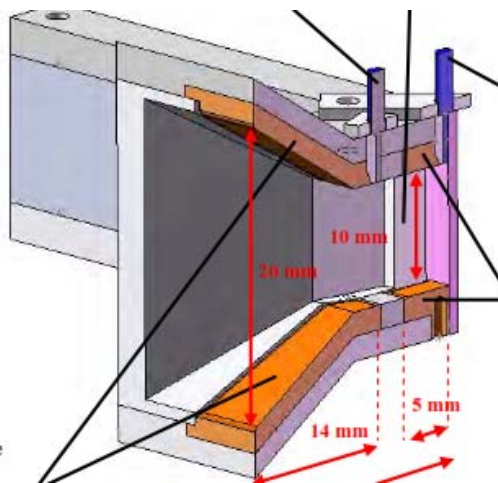


Figure 4: Flanged plate PPT configuration (Marques et al., 2009).

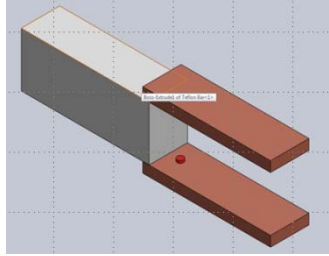


Figure 5: Parallel plate PPT configuration.

Other configuration exists as well such as coaxial PPTs. Thrust production includes electromagnetic and gasdynamic forces for all these PPT geometries.

To generate a plasma some type of propellant needs to be used to create an ionized gas. The propellant of choice in PPTs is typically Teflon[®] however H₂O (water) PPTs have been investigated by John Hopkins APL, WPI and Busek Co. Inc (Partridge, 2008). Additionally, some PPTs ablate their own electrodes as propellant (Lapas, 2009).

A PPT is an electromechanical system because electromagnetic fields and aerodynamics effects both contribute to the thrust production. However, the PPT can be modeled as a purely one-dimensional electrical circuit through the lumped circuit model. The lumped circuit model considers the components electrical characteristics such as resistance, capacitance, and inductance. (Laperriere et al, 2005; Laperriere, 2007) Figure 6 illustrates the lumped circuit model for a PPT.

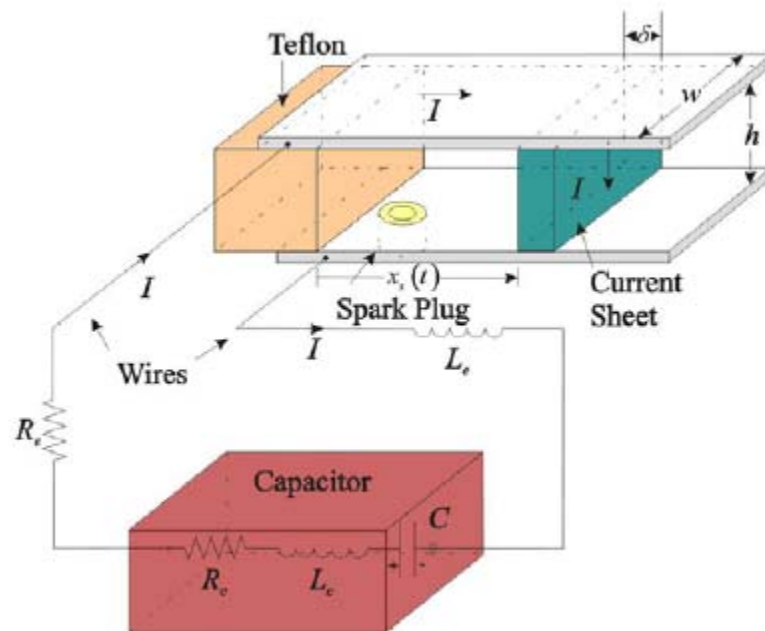


Figure 6: PPT with circuit model (Laperriere et al., 2005).

Formation of this model can be made from first principles. The electrode plates have a resistance, and an inductance. The capacitor has a resistance, capacitance, and inductance. The plasma sheath completes the circuit because it conducts a current density. This one-dimensional model can be used to determine the physical dimensions of the PPT because changing geometric properties will effect the inductance and capacitance of the L-R-C circuit in Figure 6. It is important to note that this L-R-C system is a 2nd order system and therefore 3 responses should be expected depending on the type of pulsing frequency the PPT operates in and on the component's respective impedances. You can have an overdamped, underdamped, or undamped stable system. An undamped stable system is desirable for a PPT because ringing has been known to cause late time ablation which accelerates slow neutrals and decreases the thruster's efficiency.

Up to date many PPTs have been made. The following Table 2 summarizes most PPTs that have been made to date and their respective performance characteristics.

Table 2: Flight Proven PPT's and characteristics

Mission Name	Satellite	Pulse Frequency (Hz)	Pulse Period (sec)	Capacitor Energy (J)	Input Electrical Power (W)	Maximum	Thrust Cost (uN/W)	Total Mass	Thrust (uN)	Thrust (N)	Thrust Efficiency	Total Impulse (N-sec)	Effective		Reference
	Mass (Kg) [initial mass]					Specific Impulse (sec)		per Thruster (kg)					Max Exhaust Velocity (m/sec)		
Zond 2	925	0.5	2	50	100	410	40	5	4000		8.04	1608	1.74	4022.10	(Zhurin 1976)
LES 6	163			1.9		300	17	1.4	26	3E-05	2.9	320	0.82	2943.00	(Vondra 1971)
SMS	627	1.83	0.55	8.4	15.37	400	15-20	4.1	230.55 to 307.4		3 to 4	1720	4.7	3924.00	(Guman 1973)
LES 8 & 9	454			20 to 80		1450	15 to 19	6.7	650	7E-04	7 to 13	7300 to 42700	24	14224.50	(Burton 1998)
TIP-II	170	1.5	0.67	20	30	850	19	7.1	570		7.8	4400	26	8338.50	(Burton 1998)
NOVA	170			20		543	20	6.8	378	4E-04	5.31	2450	14.4	5326.83	(McGuire 1996)
ETS-IV	640			2.3		300	13	6.6			1.92	8.83	0.02	2943.00	(Hirata 1981)
37min Parabolic	N/A			4		280	16	2.8			2.3	803		2746.80	(An 1981)
EO-1	566	1	1	8.5 to 77.6	8.5 to 77.6	1400	10.7 to 11	4.95	860	9E-04	3.4 to 7.6	1500	2.65	13734.00	(Zakrzęski 2002)
STSAT-2	100			1.8		800	14				1.34			7848.00	(Shin 2005)
FalconSat-3	50			1.96	10	827	40.8	1.7	408		8.4	29	1.15	8112.87	(Busek 2011)

1.3 Design Objectives, Requirements, Approach and Methods

The main goal of this MQP is to design a micro-PPT and a complete micro-PPT assembly that will allow control of a 3U Cubesat as shown in Figure 7.

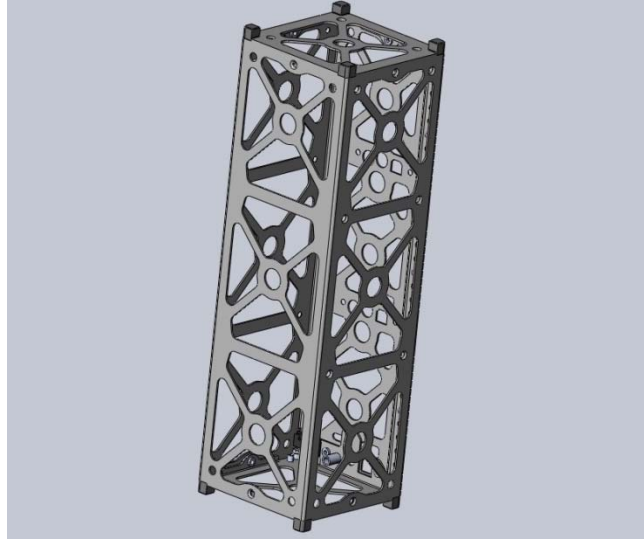


Figure 7: 3U Cubesat.

The micro-PPT design process is driven by Cubesat and mission requirements that dictate size and performance specifications. A mission’s impulse budget determines how many total pulses a micro-PPT needed. The design of the micro-PPT needs performance, geometric, electrical and material considerations. A PPT performance model (Laperriere et al., 2005) is used in conjunction with a PPT ablation model (Gatsonis et al. 2007; Stechmann 2007) to provide the basic operational requirements for the design. Table 3 illustrates a sample of the inputs and outputs from the performance and ablation models.

Table 3 Typical Performance and Ablation Parameters of the micro-PPT (Stechmann 2007).

Stechmann Model	Inputs	Units		Output	Units	
	l	m	0.036	T	K	1230
	t_{total}	s	10	\dot{m}_{max}	kg/m ² /s	2.89E+01
	t_{pulse}	μ s	8.00E-07	Find	Units	
	$t_{char\ pulse}$	μ s	5.00E-07			
	q	W/m ²	5.86E+09	m_{bit}	kg	1.19E-09
	T_j	k	295K			
	Material Prop.	p.76				
Performance Model	Inputs	Units		Output	Units	
	h	m	0.0165	$V_{exhaust}$	m/s	6613.039
	w	m	0.005	I_{sp}	s	674.3423
	l	m	0.036	I_{bit}	Ns	7.87E-06
	m_{bit}	kg	1.19E-09			
	$\rho_{electron}$	1/m ³	1.00E+21			
	$t_{char\ pulse}$	μ s	5.00E-07			
	C_{cap}	F	7.60E-07			
	L_{cap}	H	1.80E-08			
	R_{cap}	Ω	4.10E-03			
	V	V	8.00E+02			

As seen from Table 3, output parameters such as $V_{exhaust}$, I_{sp} and I_{bit} can be attained from the performance model inputs of height, width, capacitance, inductance, and resistance.

1.3.1 Mechanical Design and Structural Analysis

Mechanical Design Requirements

1. The micro-PPT must fit within 1U of a Cubesat (10x10x10 cm).
2. The micro-PPT assembly needed for attitude control must fit within 1U.
3. Material selection must meet necessary parameters for each part of PPT.
4. Electrode must have high conductivity to generate arcing.
5. Electrodes must be resistant to sputtering.
6. Housing material must resist Teflon ablation temperatures.
7. Materials must have appropriate resistive, capacitive, and inductive properties so ringing and late time ablation effects are mitigated.
8. The micro-PPT must be able to withstand vibrational loads as outlined in the NASA GEVS document (NASA Goddard Space Flight Center 2013) for spaceflight validation.

Mechanical Design and Structural Analysis Approach and Methods

1. Use SolidWorks to perform mechanical design of a single micro-PPT unit though an iterative approach.
2. Use SolidWorks to perform integration of the micro-PPTs assembly into the 1U assembly.
3. Use SolidWorks and previous CAD model for a 3U (Martinez et al. 2013) to integrate the micro-PPT assembly into the 3U Cubesat.
4. Perform material selection for electrodes and housing.
5. Perform vibration analysis using ANSYS on a single micro-PPT to meet load required in NASA GEVS document

1.3.2 Electrical Design and Analysis

Electrical Design

1. The electrical design must have 8 vacuum arc ignition systems that receives 1W - 19W input instantaneous power at voltage levels of 3.3V or 5V.
2. The vacuum arc ignition systems needs to generate a timed initial 1500V pulse that ablates the Teflon[®] surface and ionizes it.
3. The vacuum arc ignition systems needs to generate main 750V timed pulse to begin current conduction through the plasma so that the current sheet can be accelerated by a Lorentz Force.

Electrical Design and Analysis Methods and Approach

1. Use the Clyde Spaces Power Distribution Module (PDM) as an intermediate board between the Power Processing Unit (PPU) and vacuum arc ignition system to control power and voltage levels to required values and to generate timed pulsed signals.

2. Design a two stage Marx-Bank Circuit for the initial discharge to double the voltage from an input EMCO Proportional Boost Converter to create 1500V pulse
3. Use the EMCO Proportional Boost Converter to generate main 750V pulse
4. Simulated Marx-Bank Circuit with PSPICE (Cadence 2013) to ensure functionality.
5. Created 2-D circuit schematics with MULTISIM (National Instruments 2013) and transferred drawings to ULTIBOARD (National Instruments 2013) for PCB routing and to generate 3-D models.
6. Re-rout ULTIBOARD traces to reassure 3-D models fit in the bottom 1U third of a 3U Cubesat.

1.3.3 Thermal Design and Analysis

Thermal Design and Analysis Requirements

1. Investigate the transient thermal behavior of the micro-PPT design in response to expected thermal loads.
2. Determine thermal impacts of micro-PPT during long firing periods.

Thermal Design and Analysis Methods and Approach

1. Use ANSYS and COMSOL for thermal modeling of 1D Teflon geometry.
2. Validate against known solutions.
3. Develop an input model for transient heat flux to represent the pulsed behavior of a PPT.
4. Validate the pulsed model with simulations.
5. Use the pulsed model to characterize the thermal behavior of the micro-PPT and verify the thermal design.

Chapter 2: Mechanical Design

This chapter discusses the methodology and procedures undertaken for the mechanical design and structural analysis of the micro-PPT and the micro-PPT assembly. The chapter presents the design parameters including material selection, design revisions, CAD models as well as ANSYS vibration analysis.

2.1 Mechanical Design and Requirements

Pulsed Plasma Thrusters are known for their simplicity and robust nature. Our structural design attempted to limit complexity and added more features to subsequent design iterations only when structural integrity or mission drivers deemed it necessary. The first structural design developed was a parallel plate PPT with a rectangular shaped Teflon[®] fuel bar. The initial design included an outer housing which held the teflon and electrodes together. It was scaled to fit on the centimeter scale of a 1U Cubesat. The initial design is shown below in below in Figure 7.

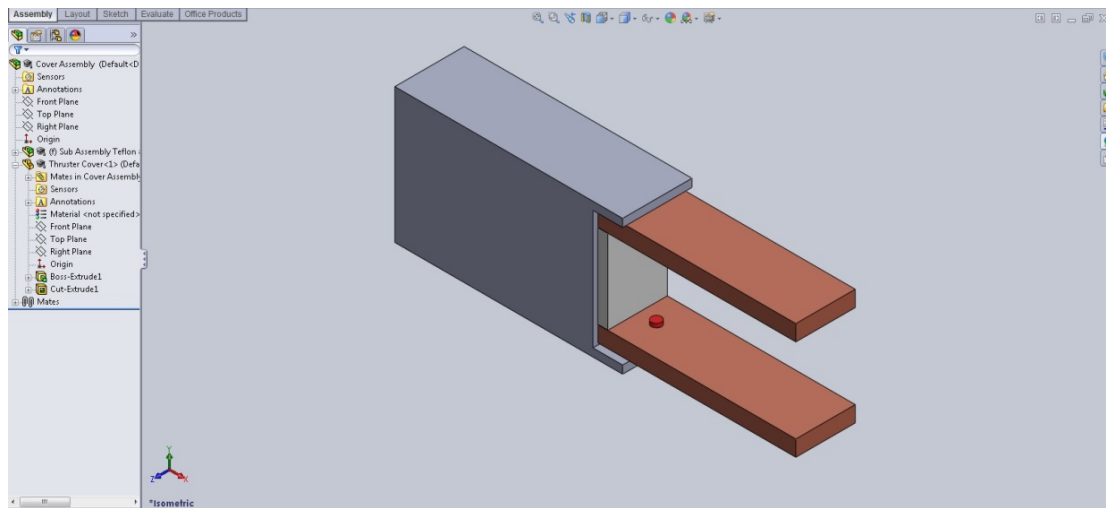


Figure 8: SolidWorks model of initial parallel plate micro-PPT design.

From this preliminary design additional modifications were made to satisfy mission drivers and improve structural integrity. The preliminary design had no specific geometric dimensions or material specifications. All sizing and material selection would be done in subsequent iterations with the help of a one-dimensional performance model (Stechmann, 2007).

Although PPTs are relatively simple electromechanical devices, the Teflon[®] ablation process is complicated. Teflon does not directly sublime when the discharge encounters it. Rather, Teflon[®] undergoes physical and chemical changes prior to leaving the surface, making

the process a highly nonlinear function of heat flux, material property variations, changing molecular weight, and phase transformation behavior. Stechmann's validated performance model provided our subsequent design iterations with expected performance characteristics for respective geometric sizes and materials.

Using the performance model (Laperriere et al., 2005) it was determined electrodes sizes less than 0.75cm thick are ideal. It was also determined an electrode surface area of 4cm² (1.25cm x 3.2cm) is ideal. Additionally, the electrode separation is a crucial parameter. The model predicted a separation of 1.5cm would provide the best characteristics.

Additionally, Teflon[®] bar sizing was determined. A Teflon[®] bar of surface area 1.75cm² (1.25cm by 1.4cm) is ideal for best performance. The fuel bar length depends on mission drivers such as impulse budget. After all appropriate sizes were determined future design iterations considered structural acceptability in the presence of vibrations. Small structural changes were made for vibrational purposes.

2.2 Material Selection

Electrode materials were investigated first. The electrode plates needed to have the following properties; low electrical resistance; high melting point; low thermal expansion; and erosion resistance. The low electrical resistance is related directly to the principle of PPT operation that requires an arc across the two highly conductive plates. Secondly, due to electrical arcing and ablation of the solid Teflon, the temperatures of the PPT will become very high and therefore the electrodes need to be able to withstand the expected temperatures. Also, as temperatures will become very high and be fluctuating we do not want the size of the electrodes to be greatly fluctuating especially at such small scales as planned for the centimeter scale micro PPT. Lastly, the ablation of the Teflon material causes ions to be accelerated out of the PPT creating thrust. That being said, these ions have the chance to impact the electrodes and impinge on them causing damage thus a material that has the ability to resist this affect would be highly desired. From these parameters previously designed PPT's were looked at for their electrode materials. From this search copper and copper alloys appeared to be the most commonly used electrode materials. From this the Granta CES Edu Pack software was utilized to explore material properties.

The review of previous PPTs include the Dawgstar (Cassady, et al), μ Lab-SatII (Kumagai, et al., 2003), and Clyde Space (Coletti et a.l, 2011) The electrodes on the Dawgstar PPT were copper (Cassady, et al. 2000). The μ Lab-SatII PPT investigated the use of molybdenum in place of their original material, brass. They found that molybdenum had similar performance properties to brass, but had significantly better erosion characteristics (Kumagai, et al., 2003). Lastly, the Clyde Space team used a 70% W 30% Cu alloy for its electrodes. The Tungsten-Copper alloy was “chosen for its low electrical resistivity and its good mechanical and thermal properties and reduced erosion rates” (Coletti et a.l, 2011).

The important qualities that were to be found from the past materials were derived from the characteristics relevant to the PPT design. The first of these was the electrical resistivity. Resistivity is a quality directly proportional to resistance, $R = \alpha \rho$, where α is a geometric proportionality constant (Resistivity, 2014). This quality is relevant to the design of the PPT since a lower resistance in the PPT circuit results in a higher current through the circuit, and fewer resistive losses, improving the thruster efficiency. Furthermore, in the PPT model presented in (Lappiere et al, 2005) the PPT circuit is approximated as a one-turn solenoid of infinite conductance. Therefore the resistance of the electrode material must be kept as low as possible so as to best match this approximation and keep the predictions of the model close to the real performance.

The thermal properties of the materials are relevant properties since the electrodes will be exposed to the hot plasma and their own resistive heat generation and must not melt, must expand as little as possible, and should have a low a thermal conductivity to stop heat conduction through the electrodes and into the surrounding material. The low thermal expansion will serve to prevent the thruster geometry, a characteristic important to the thruster performance (Pottinger and Scharlemann, 2007), from changing significantly. The low thermal conductivity will alleviate possible impact due to heat conduction to the Cubesat bus and components.

Lastly density was considered. Due to the mass requirements set by Cubesat specifications, the PPT materials should not be exceedingly dense so as to keep the thruster mass low.

Applying these key characteristics to the materials used by other teams, a set of minimum requirements for the electrode materials was created. CES EduPack (Granta, 2013) was used to

find the values for all the materials. Using that information the following values for the first selection stage were compiled as shown in Table 4 below:

Table 4: Values for initial CES selection stage.

Minimum Melting Point	1000 °C
Max. Thermal Expansion	1.68 e-5 strain/°C
Max. Elec. Resistance	6 e-8 Ohm.m
Max Thermal Conductivity	398 W/m°C

Following stage 1, stage 2 was used to select the group of materials from those who passed stage 1 with the highest melting point but a lower electrical resistivity. Figure 8 illustrates the selection.

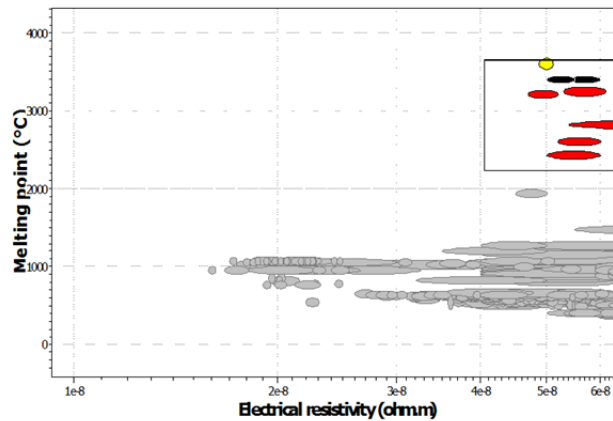


Figure 9: Results of second stage CES selection. Copyright 2013 Granta.

Following stage 2, stage 3 looked at the materials that passed stage 2 and selected a group with both low density and low price, with priority given to density as shown in Figure 9

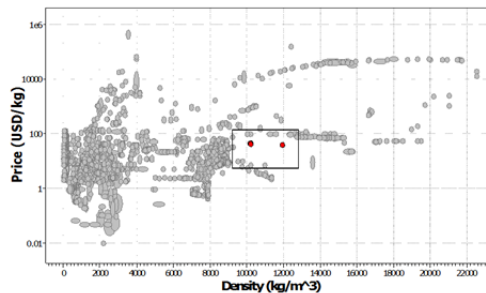


Figure 10: Results of third stage CES selection. Copyright 2013 Granta.

This final stage yielded a set off possible materials composed of molybdenum, ROSM WH8035F (a Cu-W-Ni alloy), Elkonite (a Cu-W alloy), and the 30Cu-70W alloy used by Clyde Space. A final selection was not made at that time since it was too early in the design process to do so.

Later the electrode materials selection was revisited, this time with a focus on the erosion properties of the materials. The erosion characteristics were obtained from a PPT design study by Peter Vallis Shaw in which he references a study by Fairchild Industries. The results of this study are shown in Table 5.

Table 5: Erosion characteristics of electrode materials. (Shaw, 2011).

Anode Material	Anode Erosion per discharge μg	Cathode Erosion per discharge μg
Copper	11.99	4.36
Graphite	4.59	3.17
Thoriated Tungsten	40.25	4.10
Tantalum	27.72	1.76
Tungsten coated copper	15.16	1.55
Molybdenium	16.93	3.48
25% Copper 75% Tungsten	27.81	3.86
Platinum	22.79	1.18

Due to the results of that study, and the results of the previous materials selection investigation, the final decision was that the electrode materials would be tungsten coated copper.

Next the material for the casing needed to be explored. The main parameters required for the casing are the following: good dielectric, high melting temperature, heat and electrical insulator. It is important for the casing material to be a good dielectric material to increase the charge felt across the two electrode plates creating arcing as efficiently as possible, Second the arcing and ablation of Teflon creates very high temperatures within the PPT so the casing must be able to with stand these temperatures and not fail. Additionally part of the thrust generated by a PPT is developed by the gas dynamics formed by thermal expansion. Therefore if the casing can act as a heat insulator and trap and increase the heat within the chamber it will increase efficiency of the PPT slightly. Lastly with electrical arcing taking place between the electrodes we do not want the casing material to be electrically conductive and charge the outside spacecraft bus. Once again previous PPT designs were taken in to account for a starting point.

Several PPT's used a thermoplastic material called Torlon. From this Torlon alternatives were looked at. Alternatives examined were; Tecator, PEEK, Vespel, and Techtron. PEEK is a alternative that did not have electrical properties as good as that of Torlon. Vespel had similar properties but all values were not on par however it was a very cheap alternative making it a great option for scaled testing. Techtron did not quite have the thermal properties compared to Torlon. Lastly Tecator had nearly identical properties to that of Torlon and was similar in price. However since Torlon has been a proven material to work with PPT's we decided to choose this as the casing material. Torlon 4203 properties can be seen in the Table 6 .

Table 6: Torlon 4203 Data Sheet (All-state Industries)

DATA SHEET		
TORLON 4203		
Extruded Unfilled Polyamide-imide		
PROPERTY	UNITS	VALUE
MECHANICAL		
Specific Gravity	-	1.41
Tensile Strength	psi	18,000
Tensile Modulus	psi	600,000
Elongation (at break)	%	5.0
Flexural Strength	psi	24,000
Flexural Modulus	psi	600,000
Compressive Strength	psi	24,000
Hardness, Rockwell	-	M120
Coefficient of Friction (Dry vs. Steel)	-	0.25
Limiting PV (with #1 safety factor)	psi x fpm	12,500
THERMAL		
Coefficient of Linear Thermal Expansion	in/in/F	1.70×10^{-5}
Heat Deflection Temperature (264 psi)	F	532
Glass Transition Temperature	F	527
Continuous Service Temperature	F	500
Thermal Conductivity	BTU/in/hr.ft.F	1.80
ELECTRICAL		
Dielectric Strength	volts/mil	580
Volume Resistivity	ohm-cm	$>10^{16}$
OTHER		
Water Absorption, Immersion, 24 hrs.	% by wt.	.4
Water Absorption, Immersion, Saturation	% by wt.	1.7
ENGINEERING NOTES:		
* Neat resin		
* High Purity		
* Excellent Creep Resistance		
* Good Chemical Resistance		

Once the main materials had been selected the design process was revised and it became an iterative process of changing parameters with many design revision.

2.3 Design Iterations

The micro-PPT design process consisted of various iterations that created a finalized system, which met mission requirements. Various electrode and casing geometries were examined to build a compact system that could withstand vibrations.

For the casing, various structural designs were considered to best house the components. The design needed a mechanism to feed the Teflon[®] continually into the electrode chamber. To avoid complications of moving parts, a spring mechanism was integrated with the casing to feed the Teflon[®]. The final design needed a casing-spring and Teflon[®] assembly that were structurally compatible.

The structural design initiated with the electrodes. Initially, the electrode was designed as a flat plate with a notch. The notch held back the Teflon[®] to prevent it from sliding out. Figure 10 illustrates the notched flat plate design:

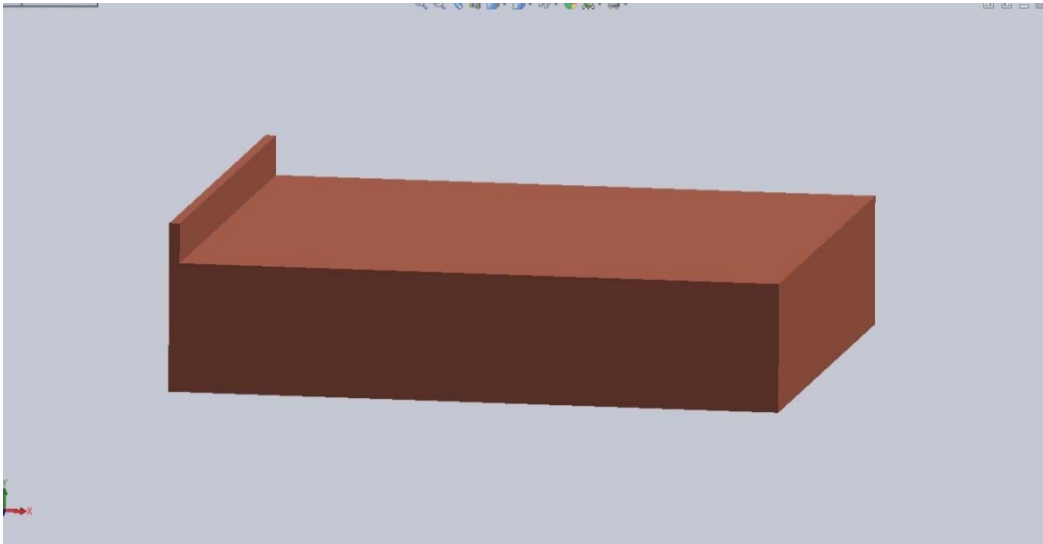


Figure 11: Flat notched electrode plate.

However, this small notch in the electrode causes localized arcing. The localized occurs at the notch because the electric field is most intense at this point. Electric field is inversely proportional to distance. The raised notch shortens the distance causing the highest potential to occur at the notch. Therefore, arcing forms at the notch. Eventually the arcing breaks down the notch and the Teflon[®] bar slides out.

In the next design iteration, a new electrode plate with an L-shaped cross section was designed. The varying thickness of an L-shaped cross section creates a slit from which the Teflon[®] bar cannot slide out. This version of the electrode is shown in Figure 11.

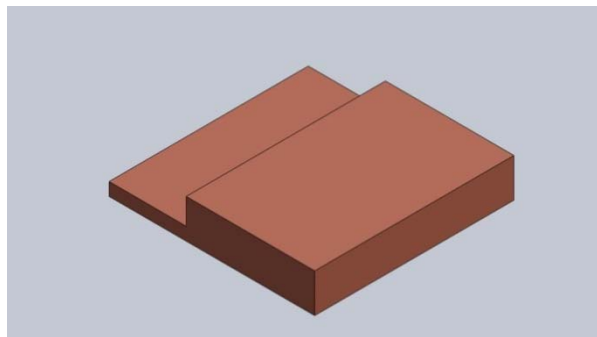


Figure 12: Electrode design with L-shaped cross section.

Although the Teflon[®] Bar could not slide out, the design did not stop the electrode plate from sliding out.

The following design iteration altered the casing itself. A notched casing that mated with the L-shaped electrode prevented all components from sliding out. The spring is mated to the back part of the casing and compresses the Teflon[®] bar. The spring force compressing the Teflon[®] is also transferred to the electrodes, pushing them against the notched surface of the casing. Figure 12 illustrates an internal view of the Teflon[®] and electrode-casing assembly being held together by the compressive force of the spring.

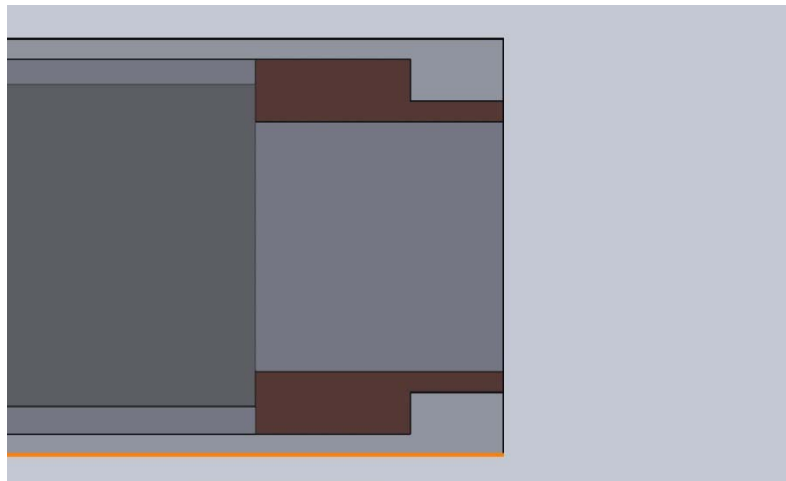


Figure 13: Teflon and Electrode-Casing Assembly Held Together by Spring Compression.

In Figure 12 the two dark brown regions represent the electrodes and the light gray around them represents the casing material. The Teflon[®] can be seen pushing the electrodes from left to right into the notched casing material.

The next design iteration focused on how to design the case-spring assembly behind the Teflon[®] bar. The case-spring assembly is a reliable design that has been proven in other PPT designs. The case-spring assembly developed utilized a sliding mechanism so the back of the PPT could be opened and re-inserted with more Teflon.

There were two case-spring assembly designs that we considered. The first attached to the main housing frame externally with the spring and Teflon pusher aligned to move through internally. The second uses a slightly larger housing to attach internally. The second option was initially chosen as the more preferred option due to its compact simple fully housed design. This design can be seen in Figure 13.

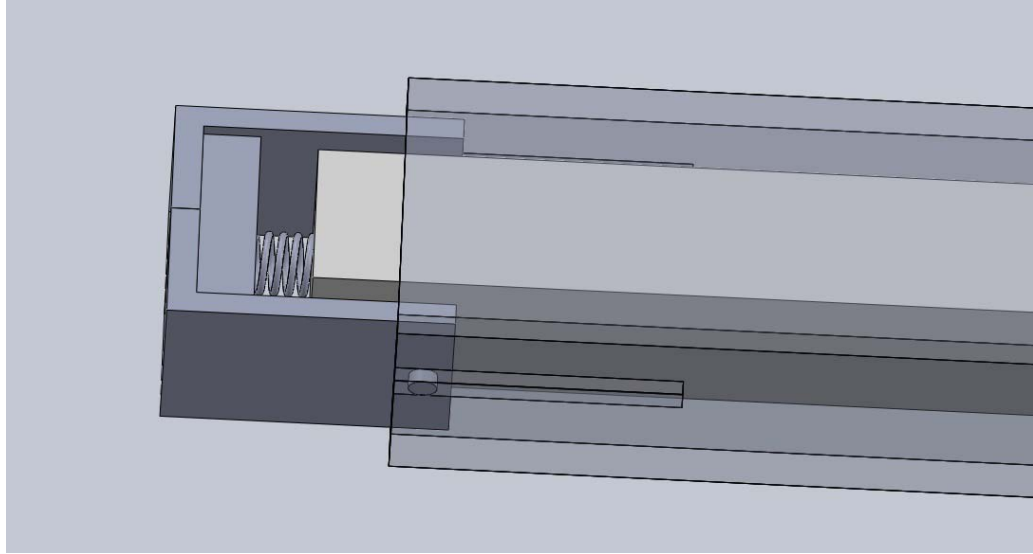


Figure 14: Initial Case-Spring Design.

In the figure above the mechanism can be seen attaching internally to the semi-transparent casing. The spring can be seen pushing the light grey colored Teflon into the PPT. At this point the first design had been produced fully and could be evaluated. The first full design can be seen in Figure 14 and Figure 15.

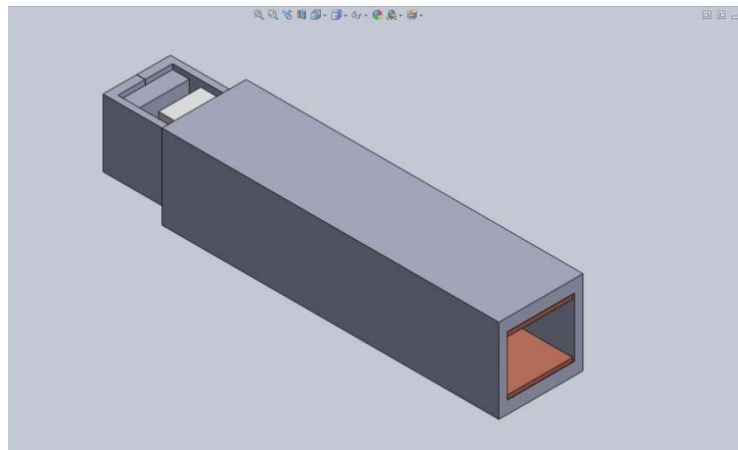


Figure 15: Completed Structural Design.

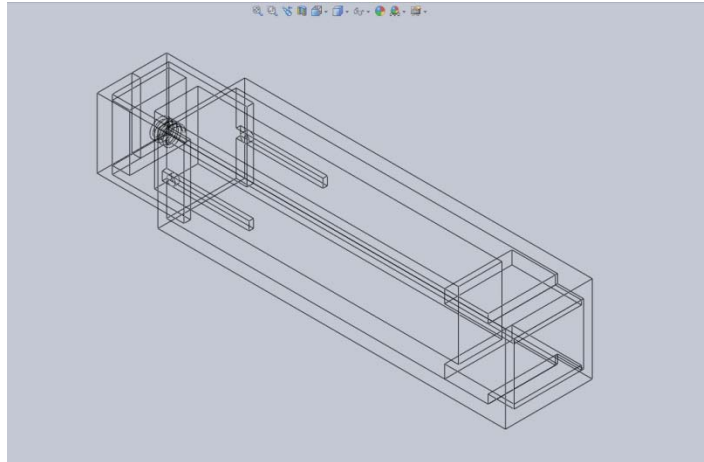


Figure 16: Internal View of Completed Structure.

As seen in the figures above this compact design solved all problems that occurred in previous iterations. The next design iteration focused on using Stechmann's performance model to determine appropriate geometric dimensions that could fit into a 1U Cubesat volume.

The PPT's geometric dimensions need to be small enough to fit in a Cubesat and allow enough space for electronics. The propulsion subsystem must all fit into 1U out of 3U available for practicality. The design is intended to provide 3-axis control for a 3U Cubesat. Therefore, thrusters and electronics which power it need to fit in a 1000cm^3 (10cm x 10cm x10cm) volume and due to the 3-axis control requirement, 8 Micro-PPTs must be included for the propulsion subsystem structure. The sizes cannot be randomly selected to allow for the smallest structure. For example, the electrode plates need to be placed at an optimal distance for best performance.

Therefore, ideal sizes were determined based of the performance model (Laperierre et al, 2005) that uses a GUI that allowed for the performance model to easily be developed as shown in Figure 16.

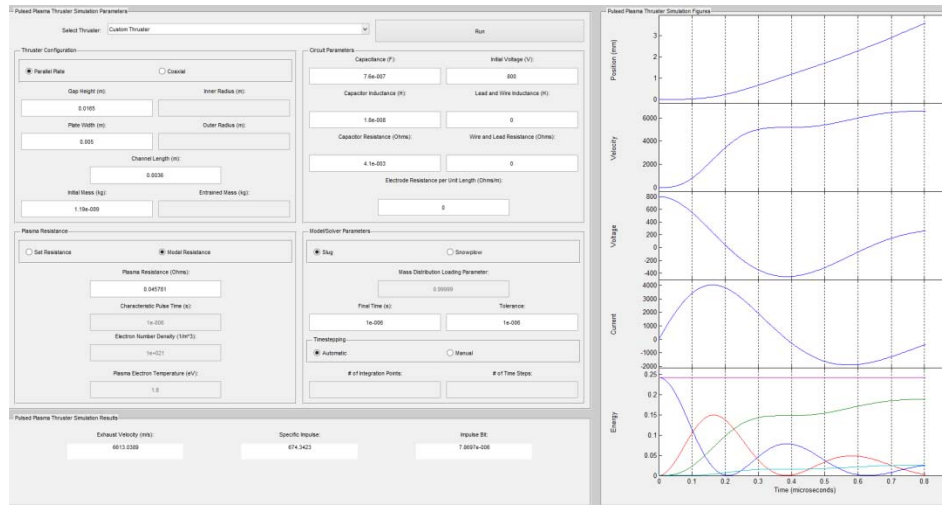


Figure 17: PPT Performance Model GUI (Laperriere et al, 2005).

From this model the ideal performance characteristics were determined. These sizing parameters determined the electrodes should be spaced 1.5cm apart, be .075cm thick, and be 3.2cm by 1.25cm. At this point the dimensions of the electrode were solidified however the model showed that a flat plate electrode with no changes in geometry would create the best performance. This along with the realization that the current design allows the electrodes to potentially vibrate and come loose made it necessary to revisit and revise the current design. This iteration of the design now set the electrode size as well as geometry, therefore the method of housing them now changed focused to how the casing could be altered to house them. A ribbed casing design was developed in which the electrodes could be slid into and be held at both the top and bottom for their entire length by these ribs. However in doing this a secondary rib needed to be made to prevent the Teflon from sliding out as the electrodes would no longer be utilized for that purpose. The new designed cover can be seen in Figure 17.

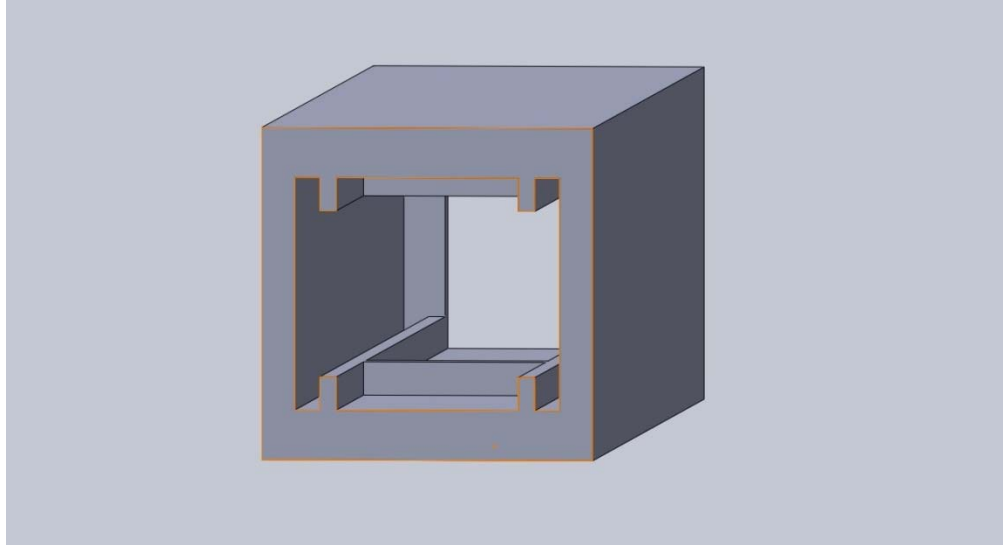


Figure 18: Alternate PPT design casing.

From the above figure lateral ribs on both top and bottom are shown. The middle horizontal rib that will hold the Teflon can also be seen. Note that this view is from the back of the PPT. Figure 18 is side by side models of front and back views with the electrodes inserted in the casing.

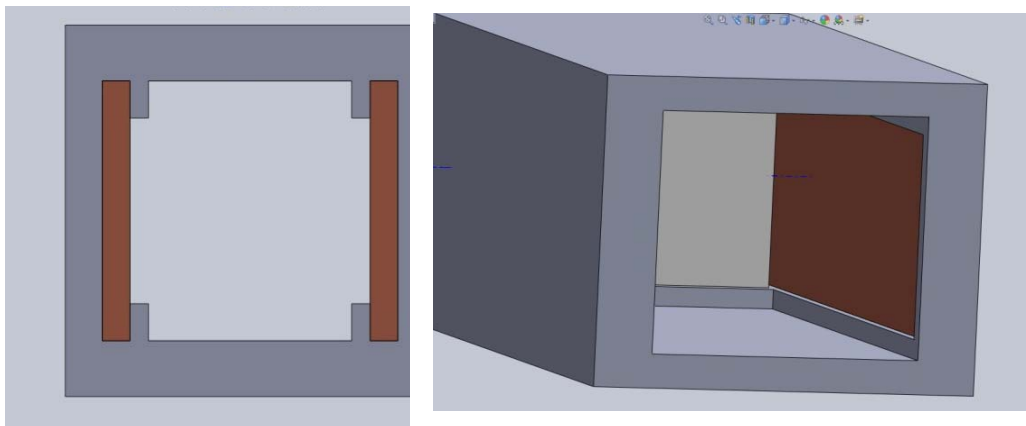


Figure 19: Front (left) and back (right) views of Alternate PPT casing.

The figures above show how the electrodes will slide in and be covered. In the front view on the left the ribs can also be seen holding in the white colored Teflon bar in place between the electrodes. This model has therefore found a secure way to house the electrons and Teflon bar. There is nothing to keep the electrodes held in on the back end. Therefore, it was determined to change the spring mechanism.

The spring mechanism was altered to be slotted into the ribs behind the electrodes. There was also a small hole added to both sides of the casing as well as a small extrusion to the spring mechanism casing so that it could slide in and be locked into position. There would then be a smaller piece attached to the spring that could push the Teflon in and slide completely internally through the thruster to ensure all Teflon will be used. This design became the finalized design and can be seen below in Figures 19 and 20.

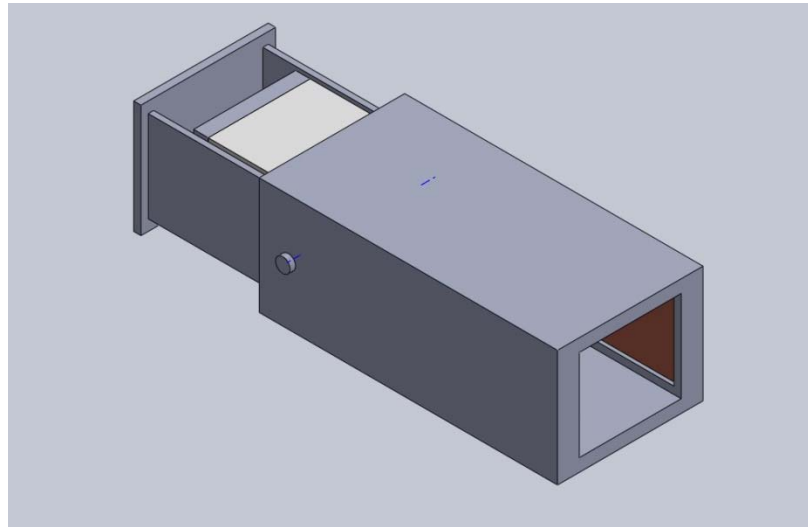


Figure 20: Isometric view of Finalized design.

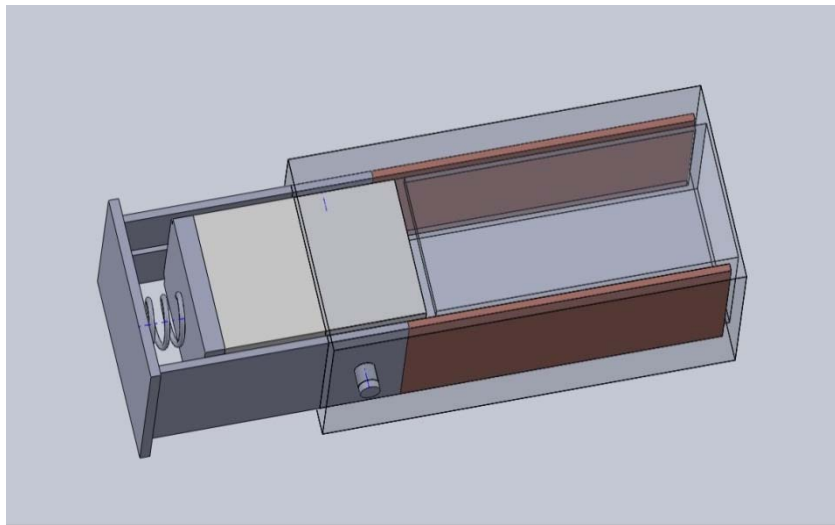


Figure 21: Final design with transparent casing to show internal portion.

From the above two figures the final design can be shown. The changes to the spring mechanism that were fore mentioned can be seen in the semi-transparent figure. From this mechanism all parts are secured, fully attached, and housed within the casing. The Teflon will be

fully used due to the internal spring mechanism which is also secured to the casing. The electrodes are fully secured and will not be able to vibrate due to the ribs in the casing and front covered area. This design has therefore been accepted as the final design.

2.4 ANSYS Structural Analysis

Once the design was finalized it needed to be analyzed, using ANSYS 14.0 software, for vibrational loads. During launch the satellite bus, and therein the micro PPT will feel a range of vibrational loads in many frequencies. In order to be space qualified NASA had produced a document stating the requirements to be considered space qualified, this document is known as the GEVS or General Environmental Verification Standard. This document provides a vibration profile requirement that can be seen in Figure 21.

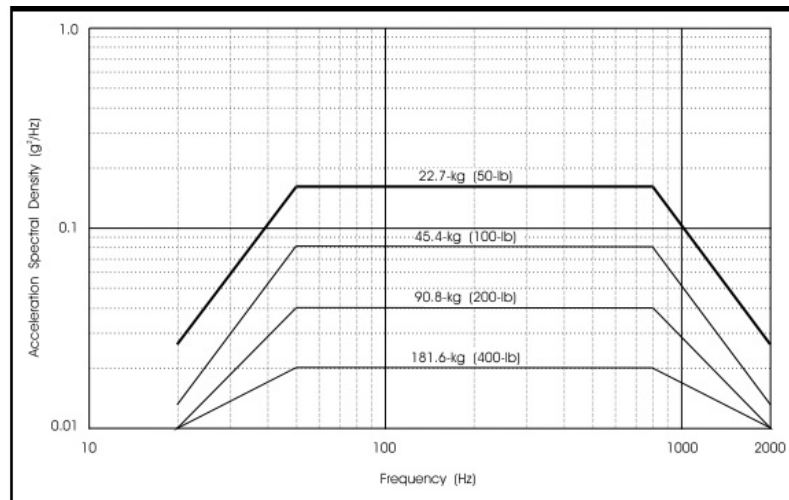


Figure 22: General Environmental Verification Standard for random vibration.

Figure 21 shows the random vibration profile for the micro PPT. The top plot will be used as the PPT is less than 22.7kg. The PPT was subjected to these loads using ANSYS. From these simulations the Von Mises stresses could be evaluated and the deformation stress tensor could be evaluated. The results are plotted on ANSYS. Figures 22, 23, 24, and 25 show the results.

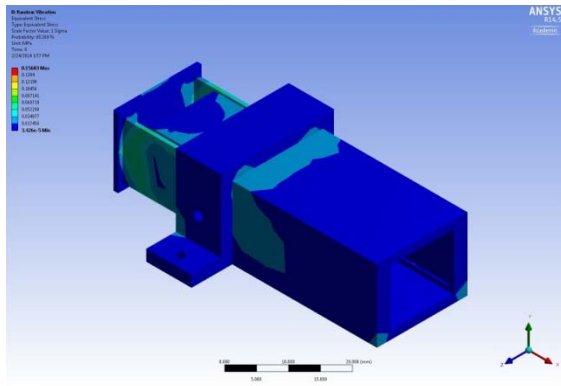


Figure 23: Von Mises Stresses from ANSYS simulation.

Figure 22 shows that the max stress is 0.15 MPa which is well within what the material of the PPT will be able to handle. It can also be seen from the color gradient in Figure 22 that most of the PPT does not even come close to that maximum value, but rather is close to the minimum value of 0.00003 MPa which is incredibly small. In Figures 23, 24, and 25 ANSYS uses the Stress Tensor to determine directional stress variations.

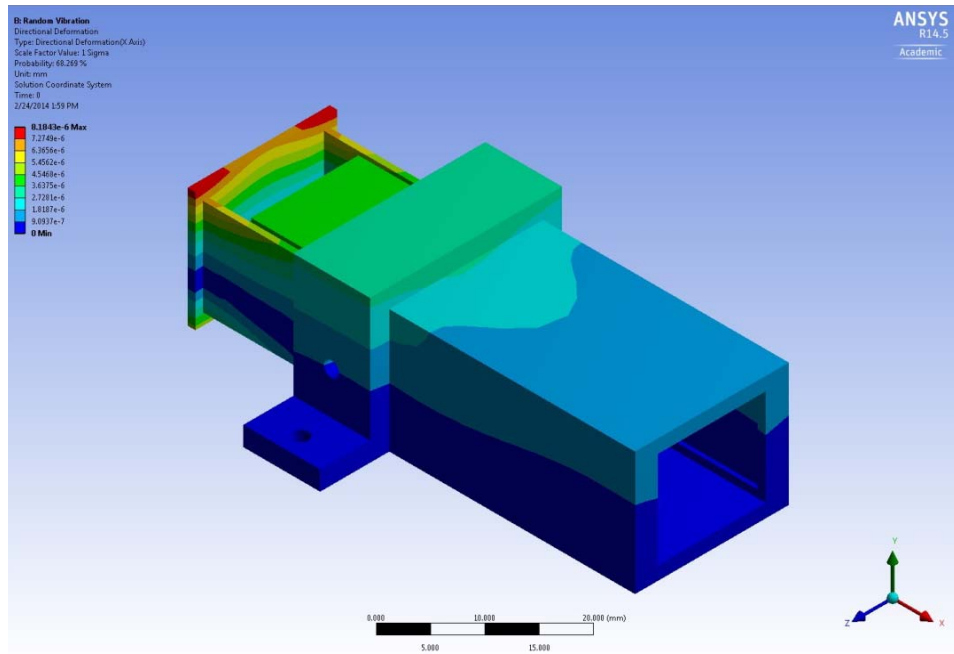


Figure 24: X-directional Deformation.

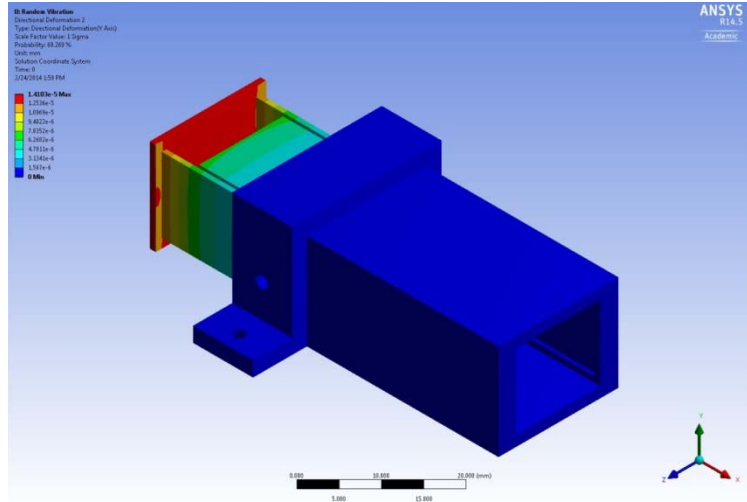


Figure 25: Y-Directional deformation.

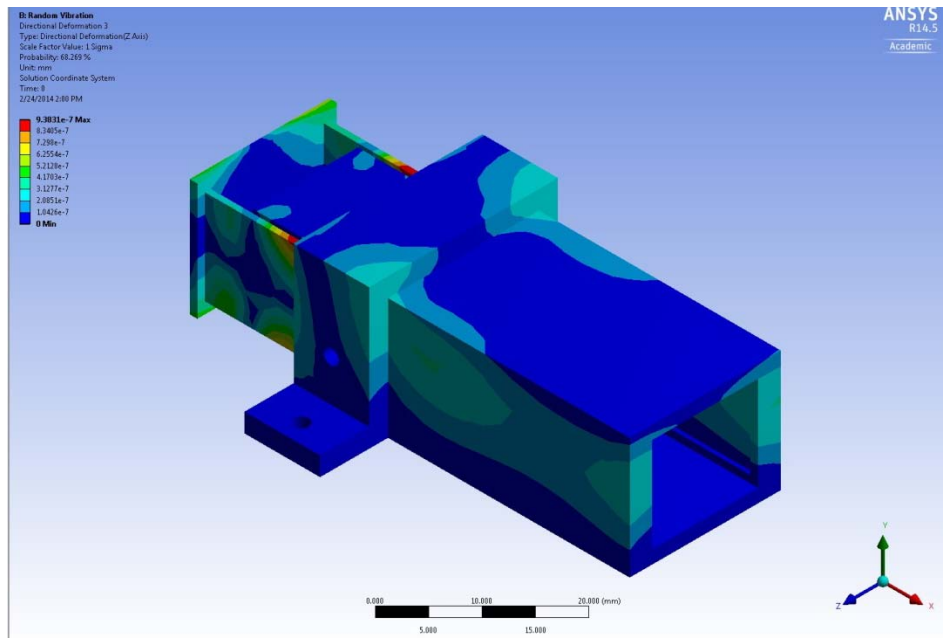


Figure 26: Z-directional deformation.

From these figures it would appear there are several regions in the red or maximum deformation areas. It can also be seen that the Y-directional deformation seems to be the most prominent. However upon closer inspection it can be seen that in Fig. 25 the red maximum areas correspond to 1.4×10^{-5} mm. This deformation is so small that it can be considered negligible. Similarly the maximum areas for the X-directional and Z-directional deformations are 8.1×10^{-6} mm and 9.38×10^{-7} mm respectively. These values are so small they can also be considered negligible. Therefore, what can be determined from this analysis is that the micro PPT has very small

stresses and deformation from the vibrations loads it would experience during launch. Therefore, the micro PPT can be considered space qualified as it complies with NASA GEVS standards.

2.5 Cubesat Integration

The micro-PPT that was designed was intended for use on a 3U Cubesat. It was decided that the bottom unit be devoted strictly for propulsion. Therefore, in that space all electronics and the 8 thrusters must be fit within the volume. Also, the structural layout of the components needs to be redundant in architecture for symmetry. This will align the center of mass appropriately and allow for stable 3-axis control. SolidWorks models for a 3U Cubesats were obtained from the 2012 Gatsonis Cubesat MQP group. Using these files the PPT could be imported into the Cubesat unit and configured to obtain stable yaw, pitch, and roll control. Figure 26 below displays this configuration.

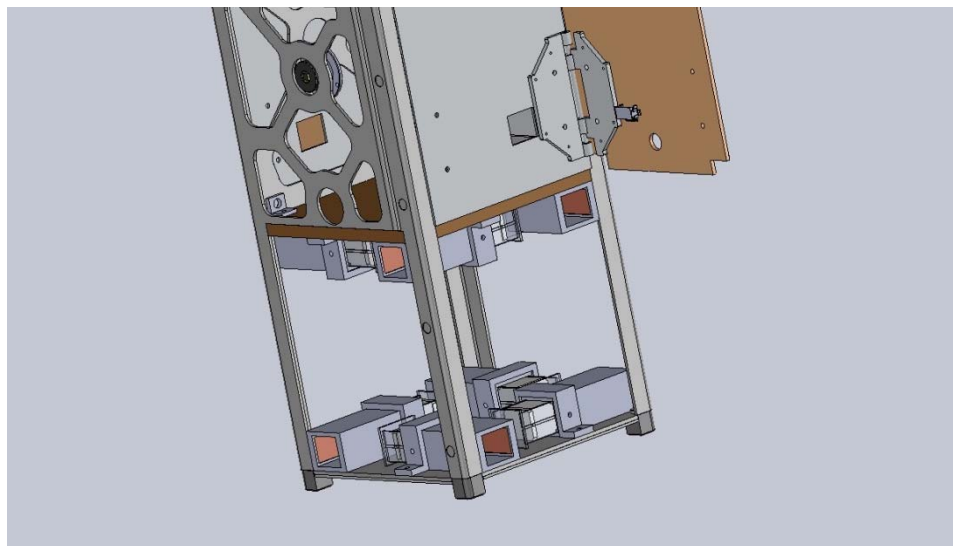


Figure 27: PPT's mounted on 1U of Cubesat.

In Figure 26 the redundant architecture of 8 PPTs is shown. Four are located on the bottom face of the unit of the Cubesat and the other four are located on the top face of the unit. This allows for stable 3-axis control. Also the top layer and bottom layer are in opposite configurations so that both clockwise and counter-clockwise spin and de-spin is possible. However, in order to place the 8 PPT's on the Cubesat the structure had to be altered slightly. Therefore, this new structure needs to be analyzed to make sure it can with stand static loads and vibrational loads experienced during launch.

Chapter 3 Electrical Design and Analysis

In this chapter we review the appropriate voltage booster circuits necessary to initiate an initial and main discharge in the electrode channel. Comparisons between different circuit topologies are provided and SPICE simulations are performed for all circuits. Additionally, the manufacturability of the circuit on a PCB board is reviewed along with proper sizing constraints of the PCB board.

3.1 Vacuum Arc Ignition System

The proper functionality of our micro-pulsed plasma thruster will depend upon the generation of an electrical arc between the two parallel electrodes. The Vacuum Arc Ignition System is responsible for creating an initial conducting path for electrons between the cathode and anode parallel plates. Field Emission is the primary mechanism for electrical breakdown in a vacuum. Field Emission is induced by an electrostatic field which causes electrons to be emitted from the cathode to the anode. Table 7 summarizes methods that can be used in parallel plate pulsed plasma thrusters for vacuum arc ignition.

Table 7: Methods for Vacuum Arc Ignition.

Triggering Mechanisms	Advantages	Disadvantages
High-Voltage Vacuum breakdown	No contamination of metal plasma	Requires a high voltage; breakdown voltage changes with electrode conditioning; Not usable for repetitive mode operation
Fuse Wire Explosion	No contamination of metal plasma	Not usable for repetitive mode operation
Contact Separation	Reliable, Simple, Repeatable	Low repetition rate; contacts may weld
Mechanical Triggering	Reliable, Relatively Simple (depending on actuator mechanisms)	Low repetition rate; contacts may weld and wear; limited number of triggering events (less than 10^4) large jitter
High-Voltage Surface Discharge	High repetition rates, reliable typically up to 10^5 pulses, low jitter	Needs high-voltage pulser; fails when approaching 10^5 pulses; plasma contamination by erosion of insulator
Plasma Injection Triggering	No Trigger Supply	Needs sufficiently high pressure in the discharge vicinity; metal plasma contamination by gas species; very large jitter
Low-voltage or 'triggerless' vacuum arc initiation	Reliable for 10^5 pulses, simple, high repetition rate possible, works without high voltage	Needs arc switch and moderate 'booster' voltage; may fail for low-melting-point and easily oxidizing cathode materials

Each system in the table above was considered as a potential candidate for our Vacuum Arc Ignition System. The ideal system would function with low voltage, possess small size and weight as to fit in a 3U volume, and be would be mechanically simple as to avoid failure due to a high repetition rate of spark firings.

A Triggerless Vacuum Arc Ignition system is most suitable for a micro-PPT because of the simplicity of the system. The system requires an arc switch and a booster voltage circuit. The device used to create the initial conducting path would be a spark plug. The voltage levels to achieve ignition are within the range of 700V-2000V. Limiting factors for a Triggerless Vacuum Arc Ignition system are the spark plug size and weight, voltage booster circuit size and weight,

and the maximum instantaneous power available from the Cubesat to supply the voltage booster circuit.

3.2 Integration of Vacuum Arc Ignition Circuit with Power Management and Distribution System

The Vacuum Arc Ignition System will receive its input power from the Power Subsystem of the Cubesat. It was assumed the power system of the Cubesat would be Clyde-Space's 3U Cubesat EPS (Part Number: CS-3UEPS2-NB). Clyde-Space's 3U EPS includes: two 8W Battery Charge Regulators (BCRs), one 3W BCR, Telemetry and Telecommand system that monitors and allows a small degree of control over the PDM stages via an I²C bus, three connection points for switch attachments for the implementation of a number of possible switch configurations, and sensors that feed commands to the I²C bus for over current and temperature protection. Clyde-Space's 3U Cubesat EPS is shown in Figure 27 and Figure 28 below:

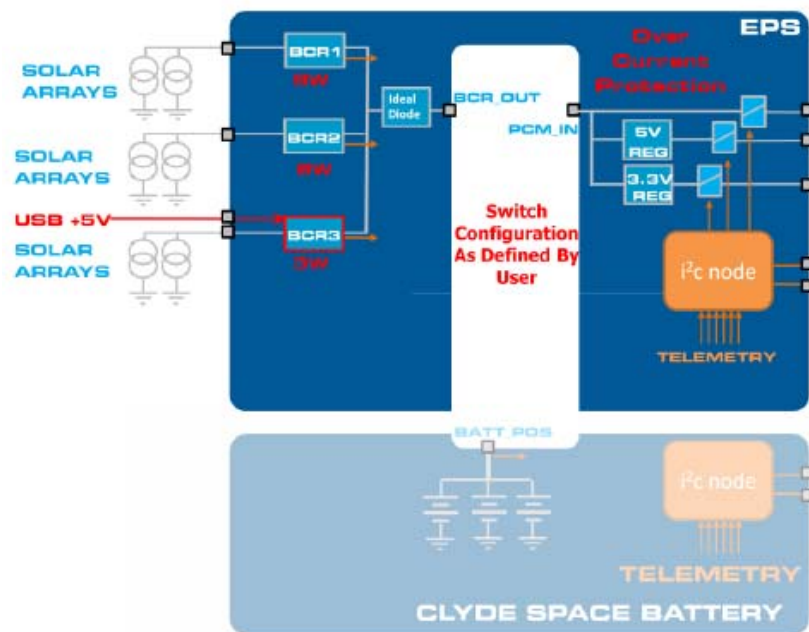


Figure 28: Clyde-Space's 3U CubeSat EPS (Strain 2010).

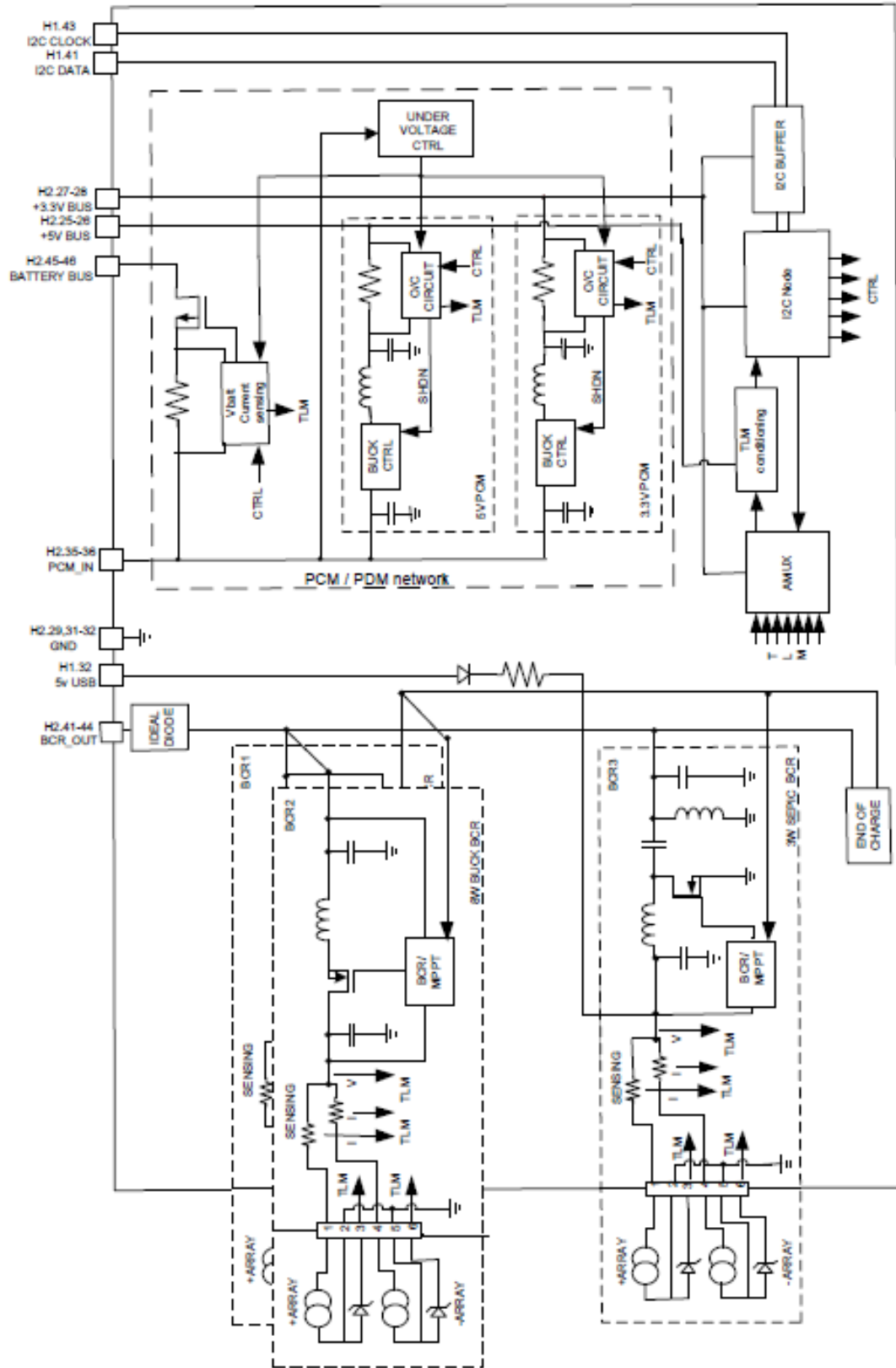


Figure 29: Clyde-Sapce's 3U CubeSat EPS (Strain 2010).

The output 5V and 3.3V signals are generated via Buck Converters that operate at switching frequencies of 470 KHz-490 KHz with a typical efficiency of 95%-96%. There are only 2 connections available for a regulated 5V output signal and 2 connections available for a regulated 3.3V output signal. Therefore, a Power Distribution Module will be necessary to interface between the Power Subsystem and the 8 micro-pulsed plasma thrusters that will be placed on the Cubesat for full range control and appropriate switching capabilities. All power buses are accessible via the Cubesat Kit header pins 25-28 as shown in the Figure 29 below.

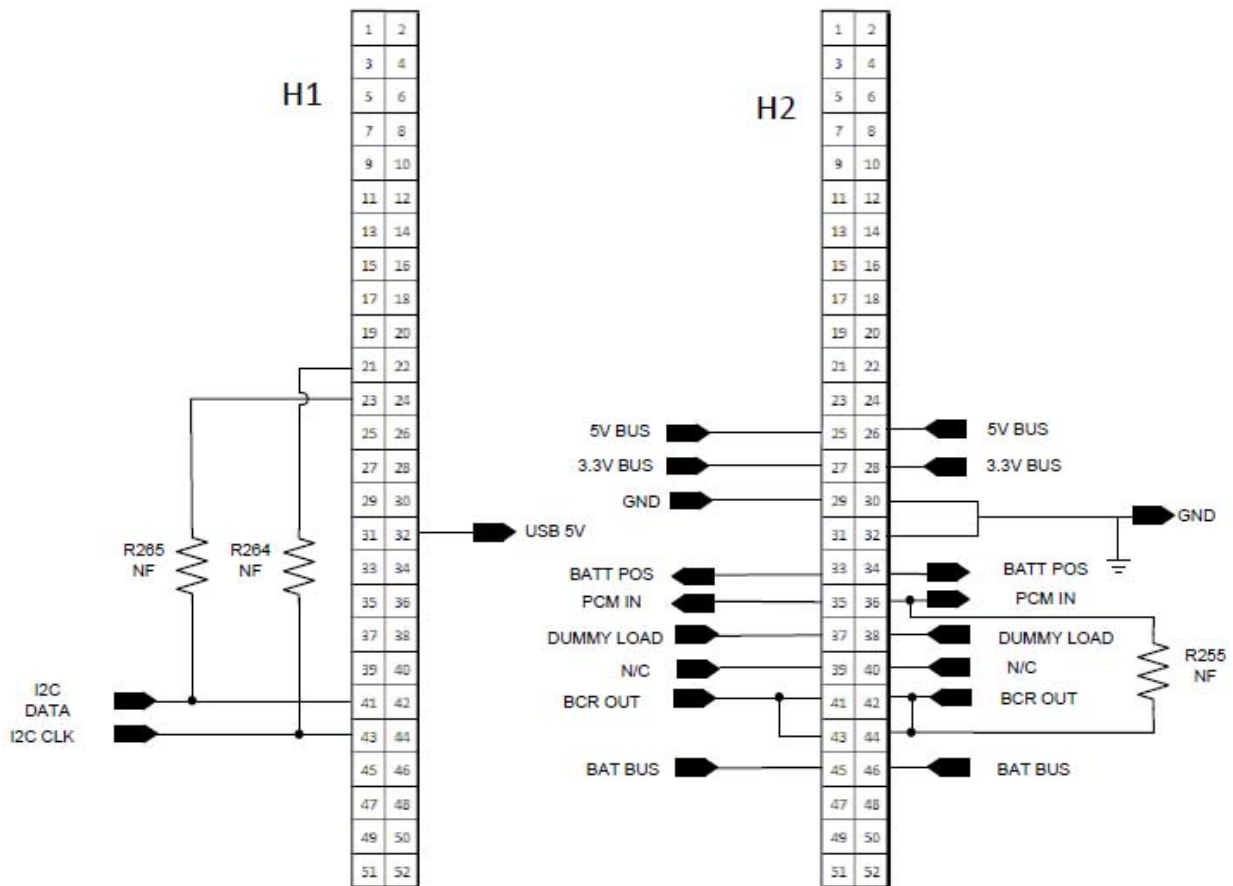


Figure 30: CubeSat Header Pins (Strain 2010).

The Power Distribution Module (PDM) would have to be connected to the header pins 25, 26, 27, and 28. The PDM of choice is Clyde Space’s Cubesat Power Distribution Module (Part Number: CN-SWT-0035-CS). This PDM has 24 power switches at 4 different voltages (3.3V, 5V, Battery Voltage, and 12V). Each switch has dedicated current telemetry, analog telemetry interfaces, and 5 RS232 to I²C interfaces suitable to integrate to a range of peripherals.

The following table, Table 8, outlines the PDMs capabilities:

Table 8: PMD Connection Capabilities.

Number Connection	Connection	Functionality
7	3.3V	Switch Lines
7	5V	Switch Lines
5	Raw Voltage	Switch Lines
5	3.3V/5V/or other voltage	Switch Lines
24	Feedback	Current Feedback lines for all Switch Lines
24	Command Ports	Needed so that all switches can be commanded on and off.
24	Status Ports	Ports so that the status of the switch lines can be provided.

The table above shows the main connections that will be made to the Vacuum Arc Ignition System. The PDM is useful because aside from allowing enough connection to the 8 micro-PPTs, the PDM will also allow for proper switching of the voltage levels via Command Ports. The On Board Computer (OBC) can be used to generate the proper On-Off logic signals. Table 9 and Table 10 give more details on the ports to connect the Vacuum Arc Ignition Signal to the Cubesat via header pin connections.

Table 9: Switch Number, Voltage level and current ratings.

Switch Number	Voltage Level (V)	Recommended Current Trip (A)
1	3.3	0.5
2	3.3	0.5
3	3.3	0.5
4	3.3	1
5	3.3	1
6	3.3	1
7	3.3	4*
8	5	0.5
9	5	0.5
10	5	0.5

Switch Number	Voltage Level (V)	Recommended Current Trip (A)
11	5	1
12	5	1
13	5	1
14	5	4*

Table 10: Header Pin Designations.

H1		H2	
1: Sw19	2: Sw19	1: Sw1	2: Sw2
3: Sw19	4: Sw22	3: Sw3	4: Sw4
5: Sw23	6: Sw24	5: Sw5	6: Sw6
7: A25	8: A26	7: Sw7	8: Sw7
9: A27	10: A28	9: Sw7	10: Sw8
11: A29	12: A30	11: Sw9	12: Sw10
13: -	14: A31	13: Sw11	14: Sw12
15: -	16: A32	15: Sw13	16: Sw14
17: A9	18: A33	17: Sw14	18: Sw14
19: A10	20: A34	19: Sw15	20: Sw16
21: A11	22: A35	21: Sw17	22: Sw18
23: A12	24: 36	23: Sw20	24: Sw21
25: A13	26: A37	25: 5V	26: 5V
27: A14	28: A38	27: 3.3V	28: 3.3V
29: A15	30: A39	29: GND	30: GND
31: A16	32: A40	31: AGND	32: GND
33: A17	34: RS232 Rx	33: -	34: -
35: A18	36: RS232 Tx	35: -	36: -
37: A19	38: Serial Rx1	37: -	38: -
38: A20	40: Serial Tx1	39: -	40: -
41: I2C_Data	42: Serial Rx2	41: -	42: -
43: I2C_Clk	44: Serial Tx2	43: -	44: -
45: A21	46: Serial Rx3	45: Battery	46: Battery
47: A22	48: Serial Tx3	47: RS422 RX A	48: RS422 TX A
49: A23	50: Serial Rx4	49: RS422 RX B	50: RS422 TX B
51: A24	52: Serial Tx4	51: Optional V	52: Optional V

As shown in the Table 10 header-2 is used for the output power connections. Specifically, 4 micro-PPTs would be run on 3.3V headers and another 4 micro-PPTs would be run on 5V header connections. Header pins 1-9 can be connected to the Vacuum Arc Ignition circuit that would run on 3.3V, and header pins 10-18 can be connected to the Vacuum Arc Ignition circuit that would run on 5V. The following equation shows how to calculate the power, P , from voltage, V , and current, I , for a circuit:

$$P = VI \tag{3.1}$$

Multiplying the voltage levels by the recommended current levels in *Table 9* determines that with 95% efficiency it is expected a maximum instantaneous power output of 1.5W – 19W assuming the solar cells could supply such instantaneous power levels.

Therefore, the design limitation of Clyde Space’s power subsystems and PDM are modular designs that house 15W-hr power availability. Power needs to be supplied via 12V lithium polymer batteries and respective solar cells to charge the batteries. The maximum power each solar cell can supply is 16W but it is crucial to take into account power losses from the solar cells to the booster circuits. Typical efficiency levels for this configuration are approximately 95% for the power subsystem and PDM.

The input to the booster circuit for the initial discharge is therefore anywhere between 1.5W-16W instantaneous power at 3.3V or 5V. The figure below is a schematic representation which gives an overview of the input power transfer from the solar cells to the spark plug or electrodes for vacuum discharge. Figure 30 below summarizes the signal flow that powers the 8 micro-PPTs we designed.

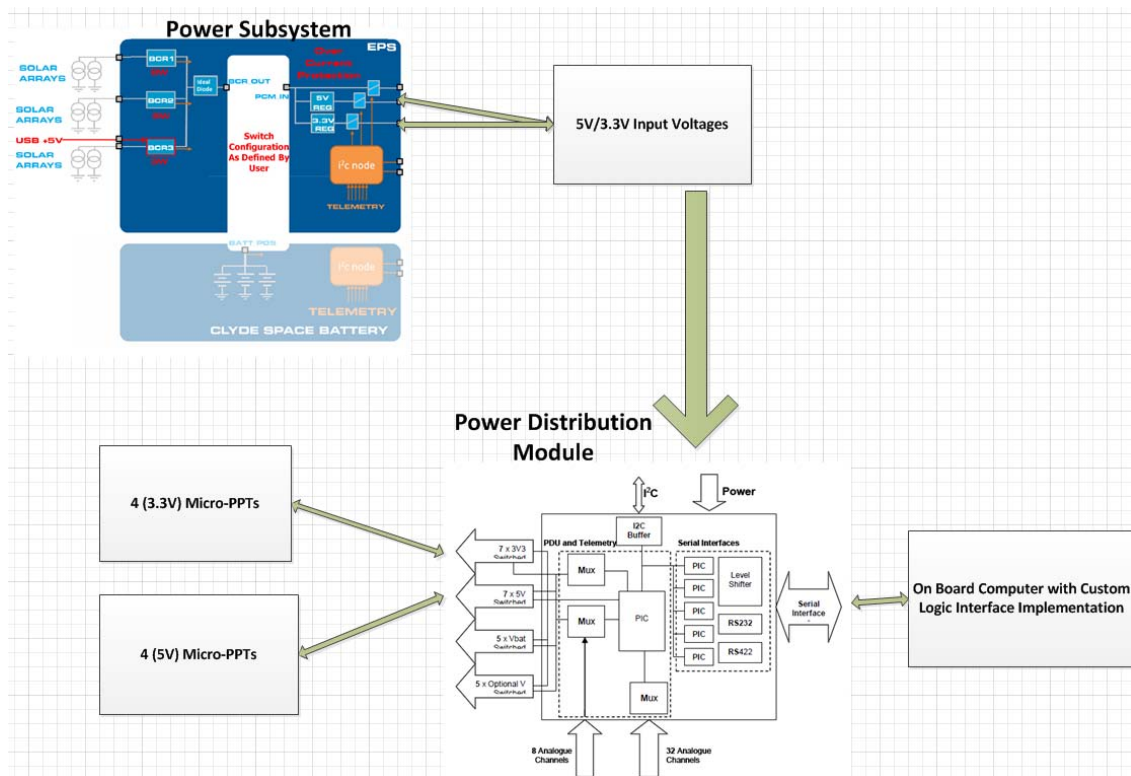


Figure 31: Signals controlling vacuum arc ignition circuit of the micro-PPT.

As observed from Figure 30, the Vacuum Arc Ignition Circuit that fires the initial and main discharges will be controlled by interactions between the Solar Cells, On Board Computer, Power Subsystem and PDM.

3.3 Vacuum Arc Ignition Circuit

It is necessary to create two main circuits for each micro-PPT that we design. One circuit for the initial discharge that will create the conducting path with the help of a spark plug and a second circuit to continue the discharge after the initial circuit are used by applying a potential across the anode and cathode electrodes. The triggering circuit for the initial discharge will be as follows in Figure 31:

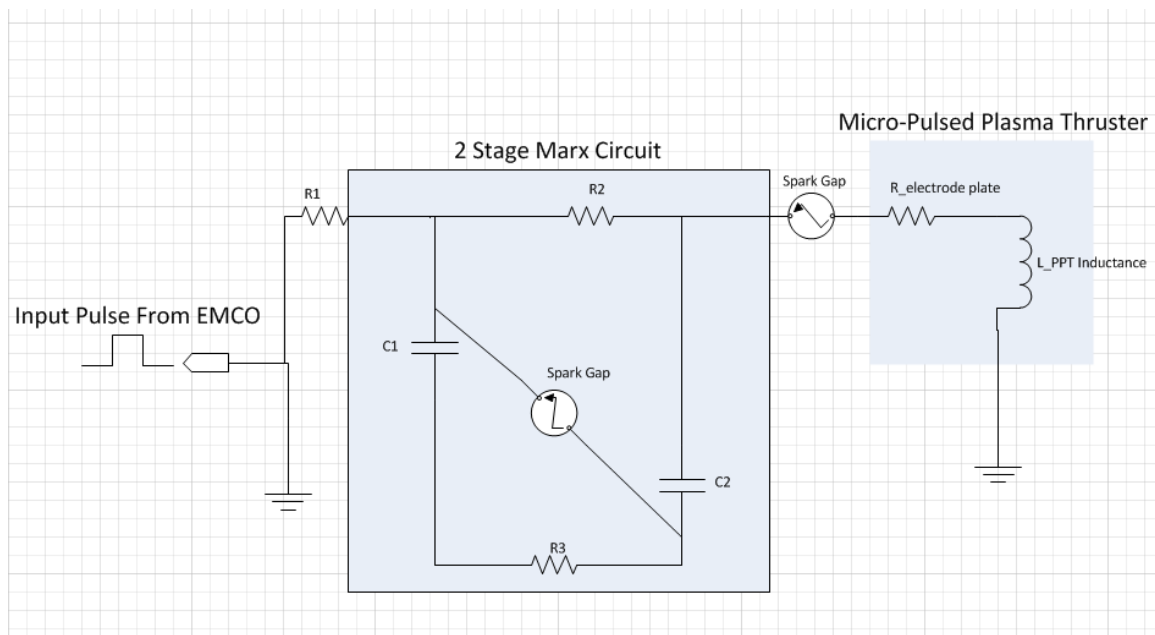


Figure 32: Initial Discharge Circuit

The circuit in Figure 31 will receive a high voltage pulse input of 750V from an EMCO G25 proportional booster as shown in Figure 32 .



Figure 33: EMCO G25 proportional booster (EMCO).

The EMCO proportional booster has the following specifications as highlight in Table 11

Table 11: EMCO proportional booster specifications.

Specification	Value
Output Voltage	0-2500V
Output Current	0 – 0.6mA
Ripple (peak to peak)	Less than 1%
Input current (no load)	Less than 125mA
Input current (full load)	Less than 275mA
Size/mass	(38.1mm x 38.1mm x 16mm) / 43grams

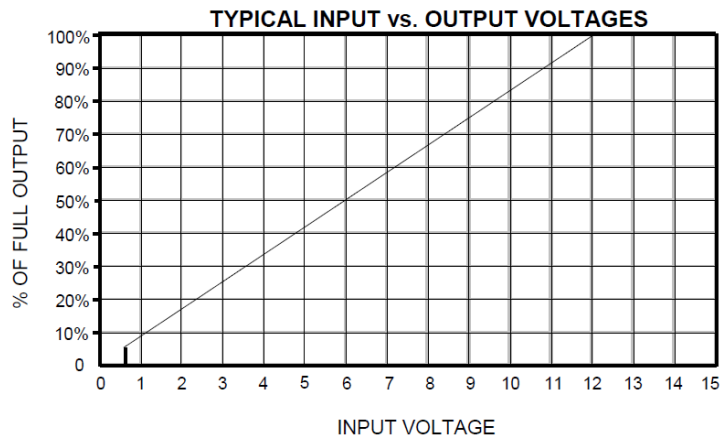


Figure 34: EMCO G25 Output voltage characteristics (EMCO).

As noted from the data above the booster is relatively small in size and can provide very high voltage values. With an input signal of 3.3V from the PDM you can expect output voltages of approximately 750V with currents of approximately 0.18mA according to Figure 33. Using Eq. 3.1 this indicates the EMCO G25 can provide a maximum of 0.135W of instantaneous power. The following pulse signal can be used to drive a power transistor to create the input pulse signal to the 2 Stage Marx Circuit as shown in Figure 34.

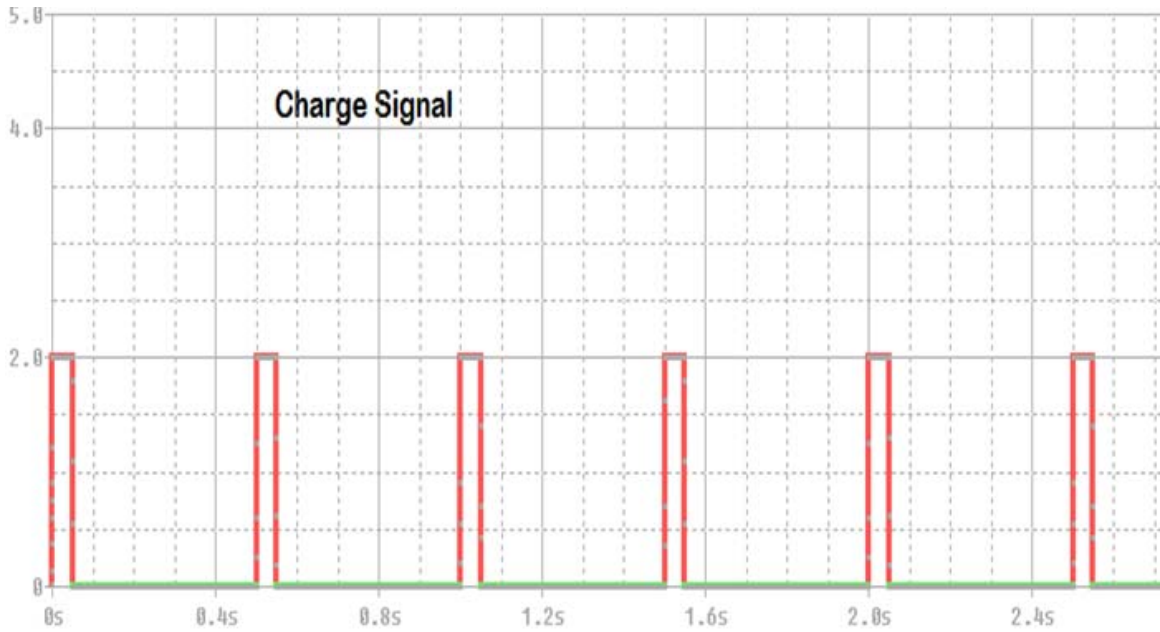


Figure 35: Input pulse signal.

This input pulse signal would drive a power transistor that would generate the required pulse. The spark gaps are to be selected such that they short out at the desired voltage that needs to be doubled. When charging the capacitors charge up in parallel to the pulse. When the spark gaps short out the resultant is a discharge in series between the two capacitors that doubles the voltage at the input. Using PSPICE the following model was created to simulate the charge and discharging of the circuit as shown in Figures 35 and 36 .

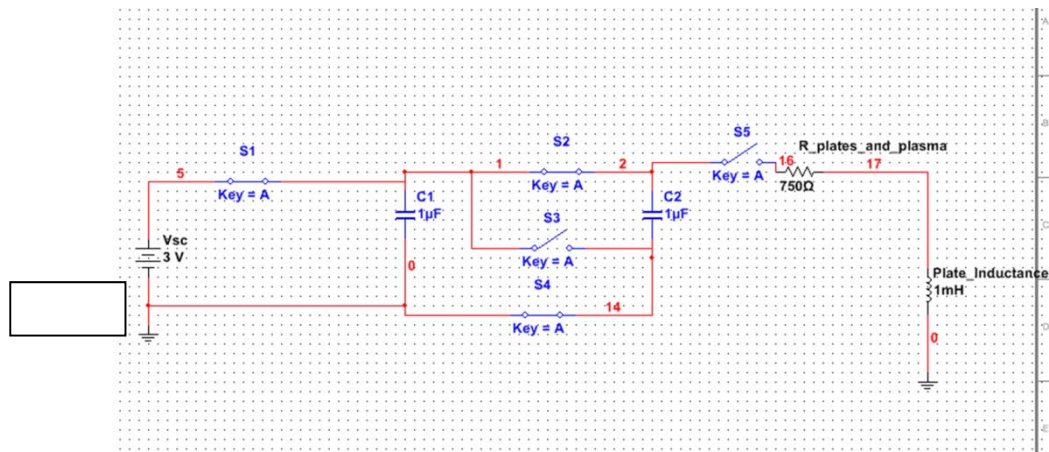


Figure 36: PSPICE circuit for simulation purposes charging configuration.

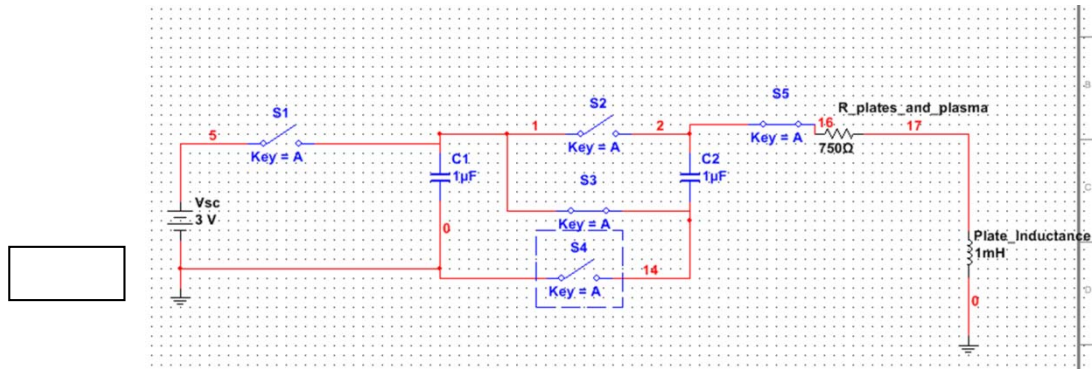


Figure 37: PSPICE circuit for simulation purposes discharging configuration.

The result of the PSPICE simulation was the following as shown in Figure 37.

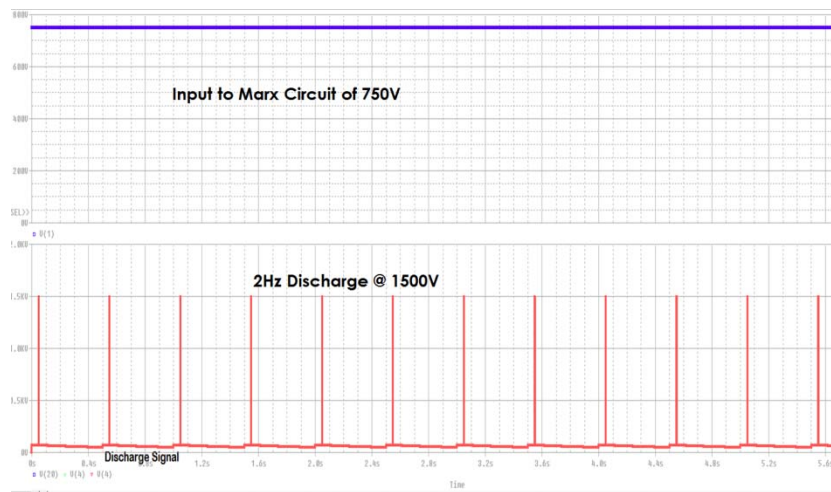


Figure 38: PSPICE marx circuit results

As shown in Figure 37 for an input of 750V that is pulsed by S1 with the signal of 2Hz, an output of 1.5KV is generated. Capacitance values of 1µF were assumed and the micro-PPT resistance and inductance values were calculated based off expected plate material properties and size.

The finalized capacitors that were selected for this circuit were custom designed CalRamic (CR2444) surface mount capacitors. This capacitor was screened to meet Mil-PRF-49467 standards with a partial discharge test at 630VRMS, 100pC Max and rated for 1500VDC. Each capacitor will only experience a max of 750V DC. The Dielectric type for this capacitor is CR09/N2200. Figure 38 illustrates the mechanical CAD drawing and specifications of the capacitor below

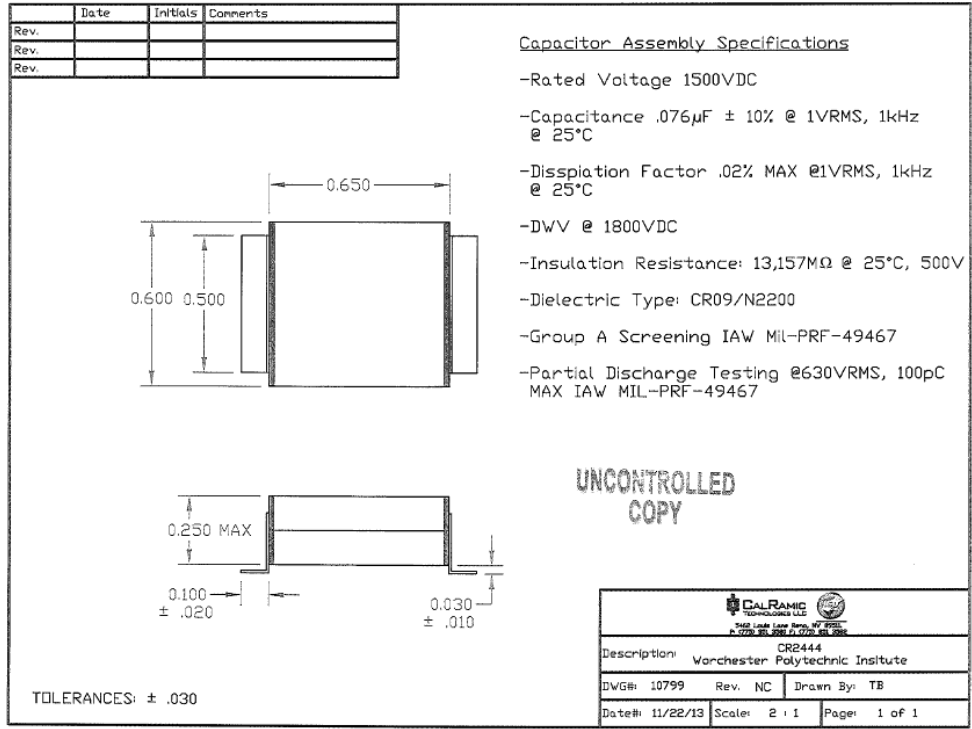


Figure 39: CalRamic capacitor specifications (CalRamic, 2013)

Figure 39, is a PCB Board drawing of the initial discharge circuit.

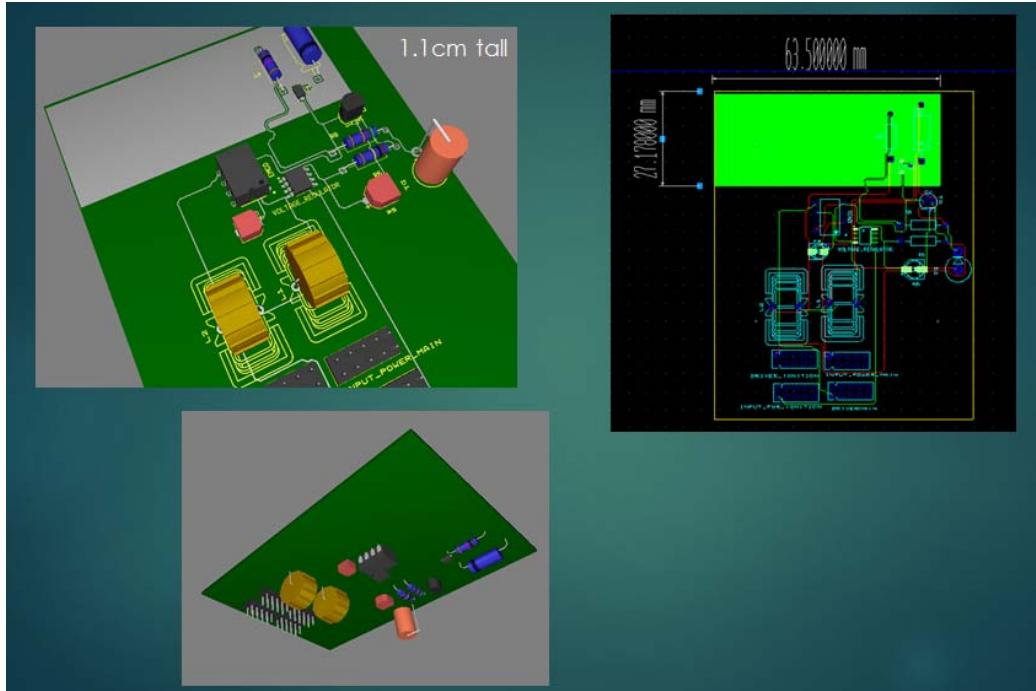


Figure 40: PCB board layout for initial discharge.

The device to generate the physical mechanism by which our discharge will initially form across the cathode and anode channel will be a spark plug. Spark plugs have the disadvantage of being large in physical dimensions but have the advantage of being reliable. Earlier PPTs including E0-1 used a Unison igniter, P/N 10390460-2, with a 0.3in diameter and outside diameter of 0.7in). A spark event can occur at any point around the circumference of its gap leading to positional variances of 0.3in relative to the PPT cathode. Therefore, by minimizing the gap length you minimize the variance of the discharge location. The smallest spark plugs found were made by Rimfire. Figure 40 shows the Rimfire Micro Viper Z3 6MM hex spark plug.



Figure 41: Rimfire spark plug (Rimfire).

However, we decided not to go along with this spark plug because discharge reliability of this park plug has been known to decrease with decreasing vacuum pressure as various experiments have shown. Unison spark plugs have been known to be reliable therefore they are

the best choice. Custom made Unison spark plugs will also have to be ordered in order to fit our sizing constraints.

The circuit of the initial discharge will not need to provide as high a voltage as the initial discharge circuit as a current path will already be created. Figure 41 highlights the signal flow for the main discharge circuit.

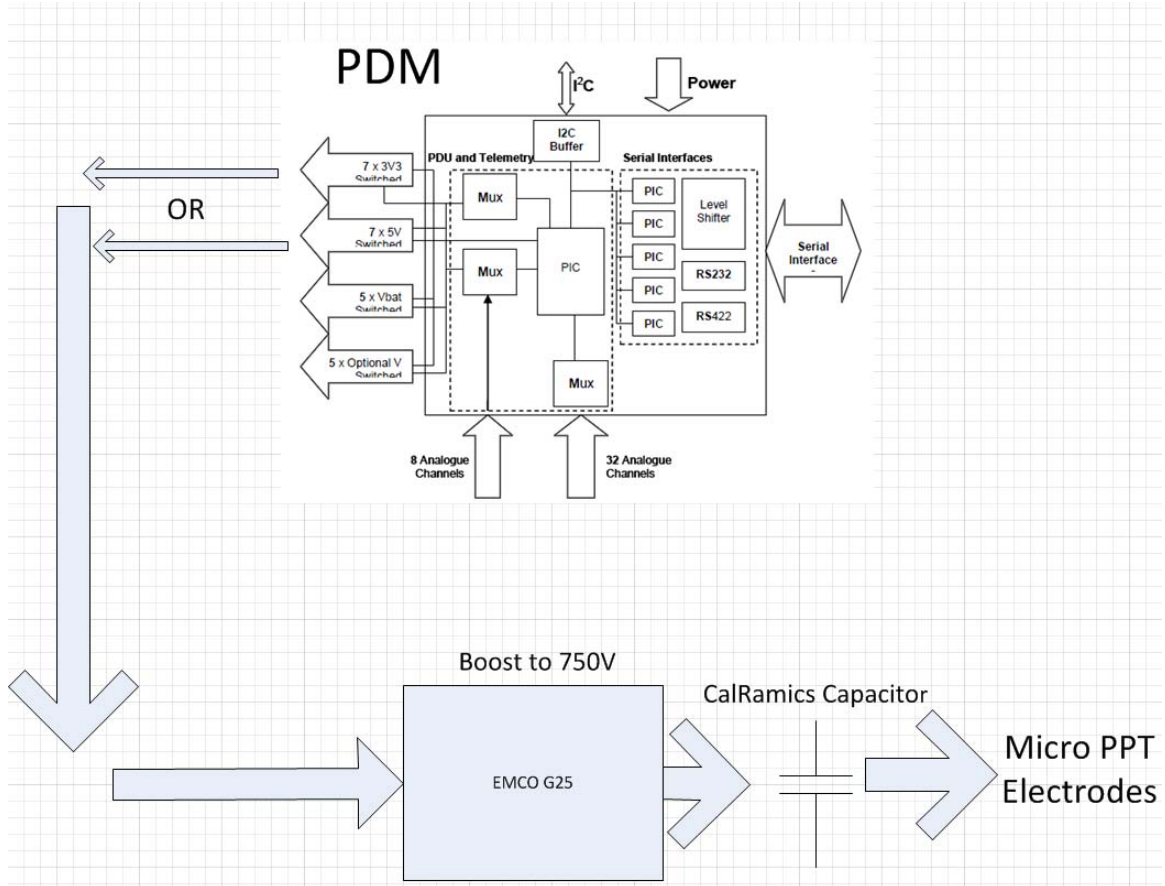


Figure 42: Main discharge circuit of the micro-PPT.

As shown in Figure 41 the same 0.076uF CalRamic Capacitor used for the Marx Circuit is adequate for the main discharge circuit. The switching will all be done by the PDM. As described in Section 3.2 the PDM has all the switching necessary to drive the pulse for the micro-PPT.

Initially we considered including the pulsing circuit as part of our main discharge circuit as shown below Figure 42.

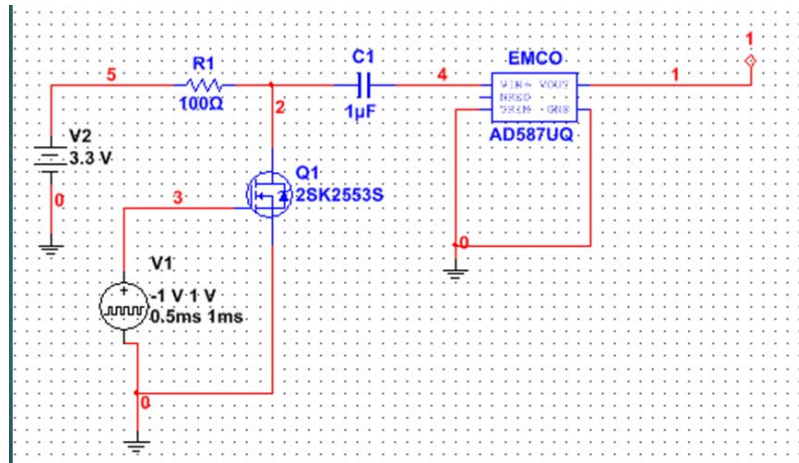


Figure 43: Main discharge initial design.

However, this is unnecessary as the PDM has all switching function already built in. Also the circuit above would have required two boards to fit all the circuitry for the 8 micro-PPTs. Figure 43 shows the PCB board with the configuration of Figure 42.

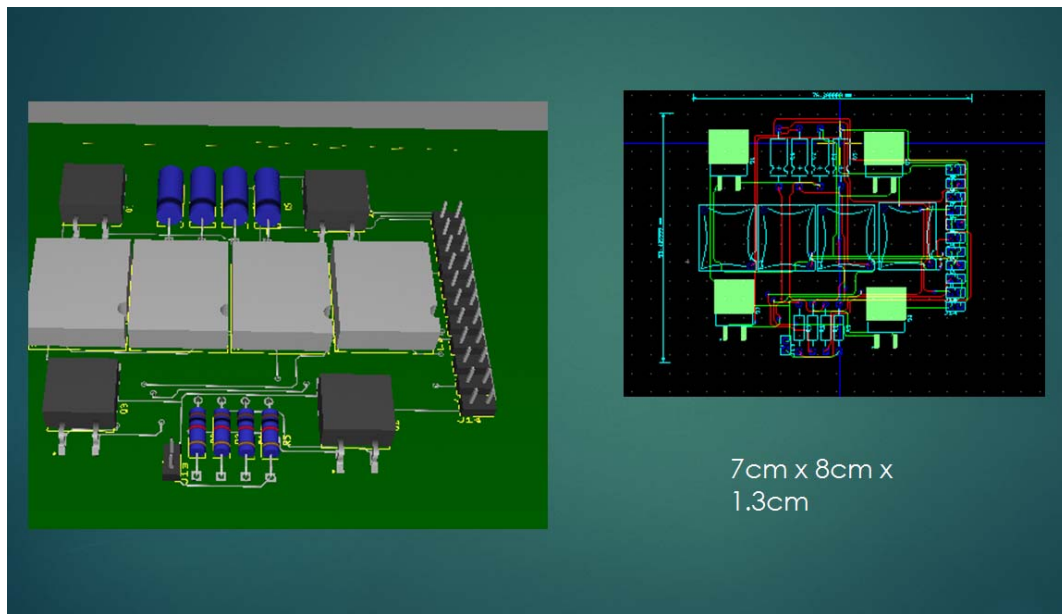


Figure 44: Main discharge PCB board layout.

Chapter 4 Thermal Design and Analysis

This chapter presents the thermal design and analysis of the micro-PPT using ANSYS and COMSOL. Validation is performed against known solutions. The process for generating a pulsed thermal input is presented and functions using the characteristics of the micro-PPT design are derived. The pulsed thermal model is validated and finally used to assess the thermal performance of the micro-PPT design.

4.1 Validation of Finite Element Analysis

Transient thermal analysis will be conducted using Finite Element Analysis software ANSYS and COMSOL. These software packages solve the transient heat conduction equations (Annaratone, 2010)

$$\frac{\partial T}{\partial t} = \frac{k}{c\rho} \left(\frac{\partial^2 T}{\partial x^2} + \frac{\partial^2 T}{\partial y^2} + \frac{\partial^2 T}{\partial z^2} \right) \quad (4.1)$$

for 1D, 2D and 3D geometries of arbitrary complexity. In order to use ANSYS and CONSOL to the thermal analysis of the micro-PPT, validation of their capabilities is performed.

The validation cases are based on those presented in work on numerical analysis of Teflon ablation (Gatsonis et al, 2005; Stechmann, 2007). In this work, a program was created to numerically calculate the rate of ablation and the body temperature of Teflon in PPTs.

4.1.1 Case 1

The first validation Case 1 that was conducted was based on Scenario One in (Stechmann, 2007). The conditions of this scenario are as follows:

- One dimensional transient heat conduction in single phase material
- Constant material properties
- Approximated as infinite length ($x \rightarrow \infty$), $x \gg 0.01$ m

Input parameters are shown in Table 12.

Table 12: Input parameters for Case 1 validation.

<u>q (W/m²)</u>	<u>T initial (K)</u>	<u>k (W/m/K)</u>	<u>ρ (kg/m³)</u>	<u>C (J/Kg/K)</u>
75900	296	0.2477	1914	707.9

The analytical solution to Scenario One is given as a solution to transient heat conduction (Stechmann, 2007):

$$T(x, t) = \frac{q}{k} \sqrt{\frac{4\alpha t}{\pi}} \left[\exp\left(-\frac{x^2}{4\alpha t}\right) - x \sqrt{\frac{\pi}{4\alpha t}} \operatorname{erfc}\left(\frac{x}{\sqrt{4\alpha t}}\right) \right] + T_{init} \quad (4.2)$$

Eq. (4.2) was implemented in MATLAB at 1, 2, and 4 seconds and at 6 different positions along the x-axis between 0 and 0.25 cm from the heated Teflon face. The same scenario was implemented in ANSYS and COMSOL, and these models were then solved for the same time periods as the analytical equation, and temperature data was then taken at the same positions as in the analytical solution. The graphical comparison of the solutions is shown in Figures 45, 46, and 47.

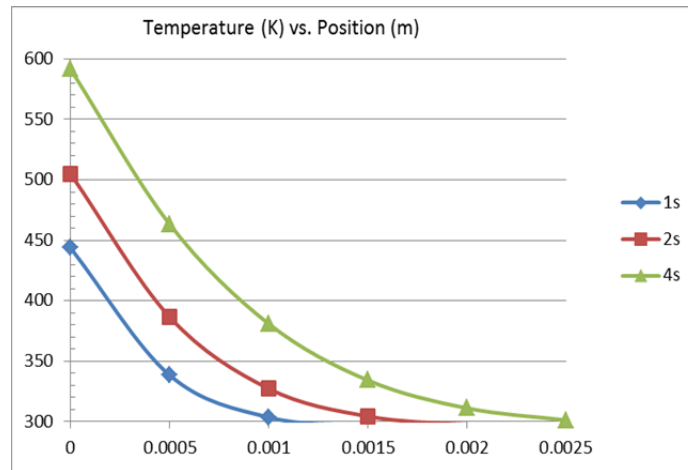


Figure 45: Analytical solution to Case 1.

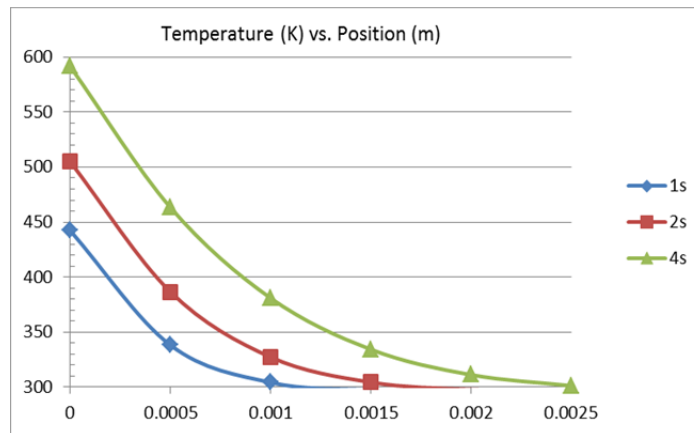


Figure 46: ANSYS solution to Case 1.

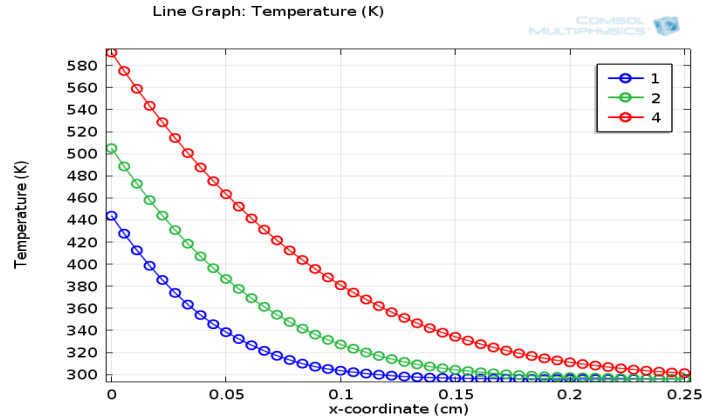


Figure 47: COMSOL solution to Case 1.

As expected, the COMSOL and ANSYS solutions are almost identical with the analytical solution for this simple 1-D transient conduction with an applied heat flux.

The second validation case was taken Stechmann (2007). In this case the ablation model is used to evaluate the operation of the XPPT-1 in various scenarios. The characteristics of the XPPT-1 model are shown in Table 13.

Table 13: XPPT-1 characteristics.

Firing Rate	1 Hz
Discharge Energy	20 J
Face Surface Area	5.29 cm ² (2.3 cm x 2.3 cm)
Initial Temperature	273 K
Propellant Domain Length	3 cm
Steel Heat Sink	1 cm

The validation Case 2 is based on the scenario conducted to produce Figure 48 (Stechmann, 2007). This involved a $7.18E8 \text{ W/m}^2$ or 4.8% of discharge power being applied in $2 \mu\text{s}$ pulses over time periods between 600 and 12000 seconds.

Initially the heat flux was applied as an average since the pulsing function would not be created until later. A time average of the heat flux was taken using the $2 \mu\text{s}$ pulse rate and the 1 Hz pulse rate to find a time averaged heat flux of 1436 W/m^2 . This profile was applied to the ANSYS and COMSOL models to produce solutions for the temperature distribution through the domain. A comparison of the solutions is shown in Figures 48, 49, and 50.

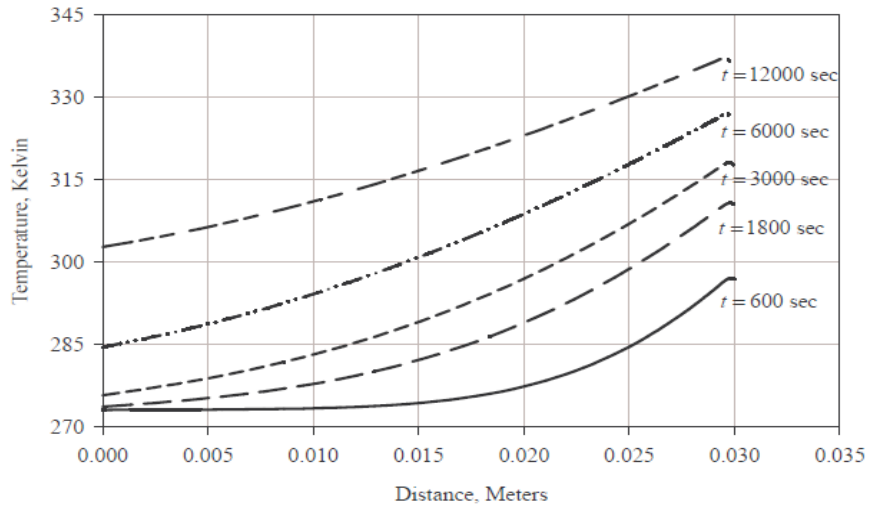


Figure 48: Temperature profile in Teflon of XPPT-1. (Stechmann, 2007)

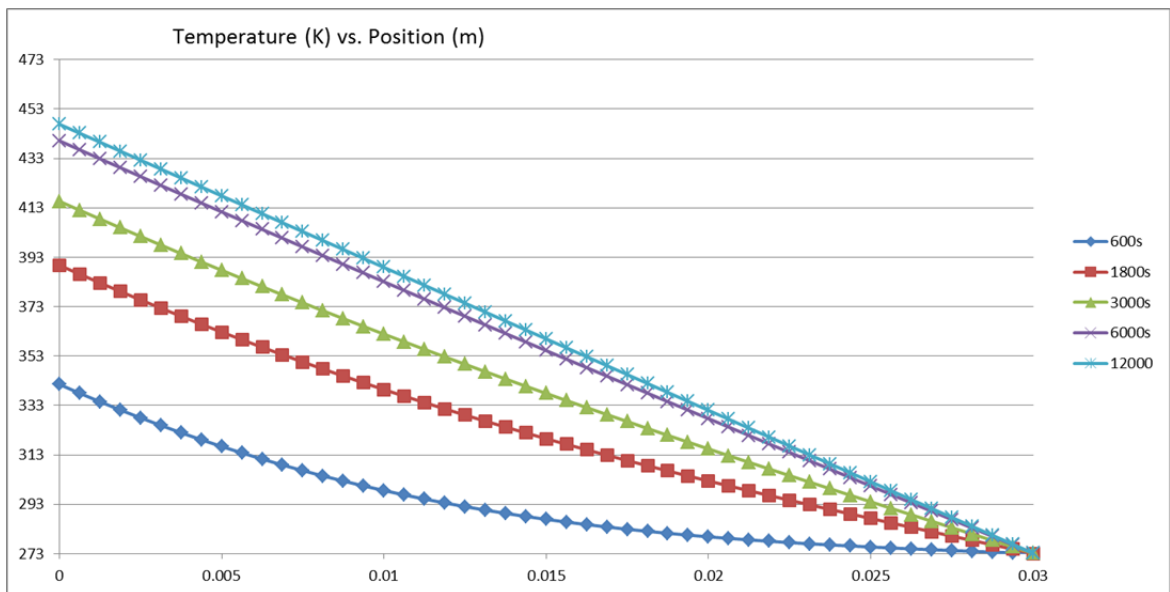


Figure 49: ANSYS solution to Case 2.

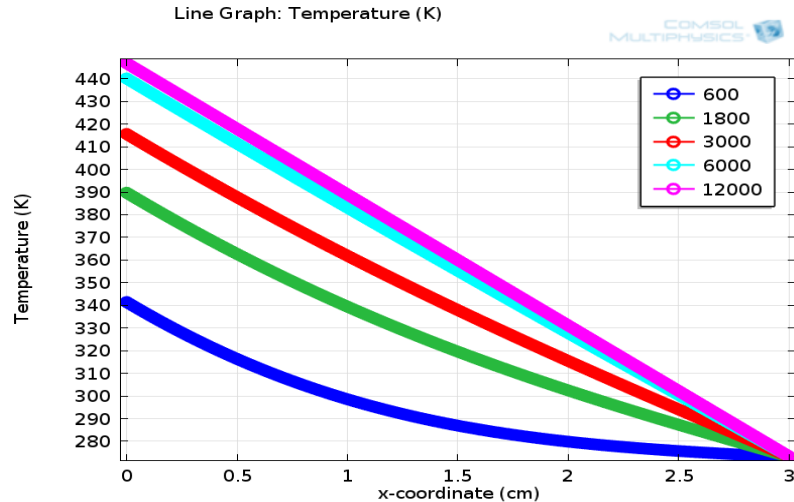


Figure 50: COMSOL solution to Case 2.

The ANSYS and COMSOL solutions are accurate to one another but show discrepancies to the solution by the numerical ablation model of Stechmann. This was assumed to be due to the fact that the numerical model takes into account the energy lost in the ablated Teflon, and since an averaged flux was used instead of a pulsed flux. The results of the validation showed that:

- ANSYS and COMSOL solutions are almost identical.
- ANSYS and COMSOL cannot fully model a PPT since it cannot account for energy loss in ablated propellant. This energy is retained and as such so these predictions will result in higher temperatures

ANSYS was chosen initially due to its more intuitive interface but COMSOL was used for the final simulations due to its greater capabilities in implementing input functions.

4.2 Pulsed Thermal Analysis

In order to run the thermal simulations a method for determining the amount of heat input to be applied to the model is needed. Since determining the temperature of the plasma between the electrodes would require modeling of the plasma as a moving body, in the FEA software a different method would have to be used.

Stechmann (2007) used a factor of 1.9-4.8% of the discharge energy in calculating the heat energy to be applied to the Teflon face in the simulations. He also quotes another study for the overall efficiency by Bushman and Burton (2001). Although this study was conducted on a different PPT configuration than the micro-PPT considered in this MQP, it did give the best analysis of heat losses in PPTs. The study found that the heat loss efficiency, η_h , was between

0.86 and 0.26 in the PPT configurations (Bushman and Burton, 2001). The efficiency was found to be dependent both on the chamber area exposed and the energy level. Higher chamber exposure and lower energy levels result in lower efficiencies and greater heat loss in the thruster (Bushman and Burton, 2001). Given the properties of the micro-PPT, a value between 59% and 75% of the discharge energy was used our analysis and the heat distribution to be used will be:

- 5% of discharge energy to Teflon face
- 70% of discharge energy to electrodes and thruster walls

To simulate the effect of the pulsed behavior, some tests with a time varying heat flux profile were conducted. This profile was taken from Stechmann (2007) and is shown in Figure 51.

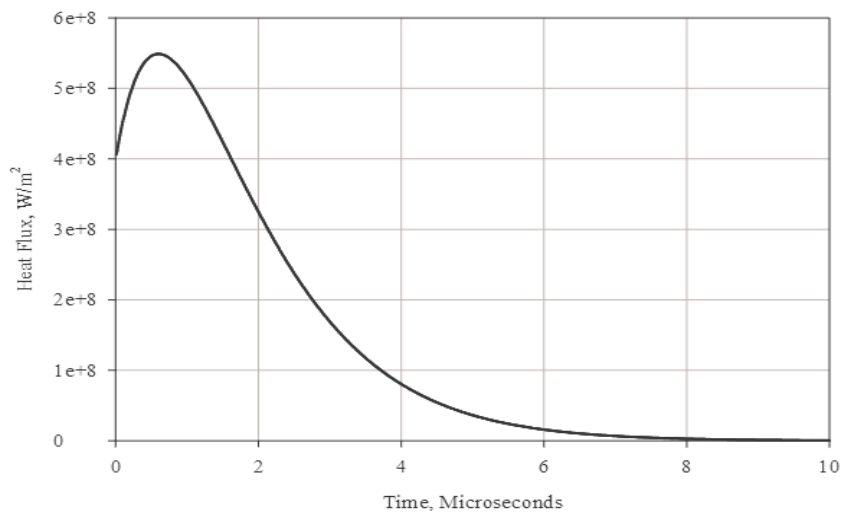


Figure 51: Time varying heat flux profile. (Stechmann, 2007)

The profile can be discretized as tabular data as in Table 14.

Table 14: Discretization of the transient heat flux profile.

Time (μ s)	Heat Flux (W/m^2)
0	4.05E+08
1	5.40E+08
2	3.20E+08
3	1.70E+08
4	8.00E+07
5	4.00E+07
6	2.00E+07
7	1.00E+07
8	5.00E+06
9	5.00E+05
10	1.00E+05

This was integrated discretely to obtain a total heat flux of $1388.1 J/m^2$. The heart flux multiplied by the area of the Teflon face presented in (Stechmann, 2007) gives a total heat

expenditure of 0.7343 J. This amounts to 3.8% of the 20J discharge energy, meaning that the discretization is acceptable. The model and conditions used in the time varying simulations are the same as in the Scenario One. The discretized profile of Table 15 was applied to the model. The COMSOL results are displayed in Figure 52.

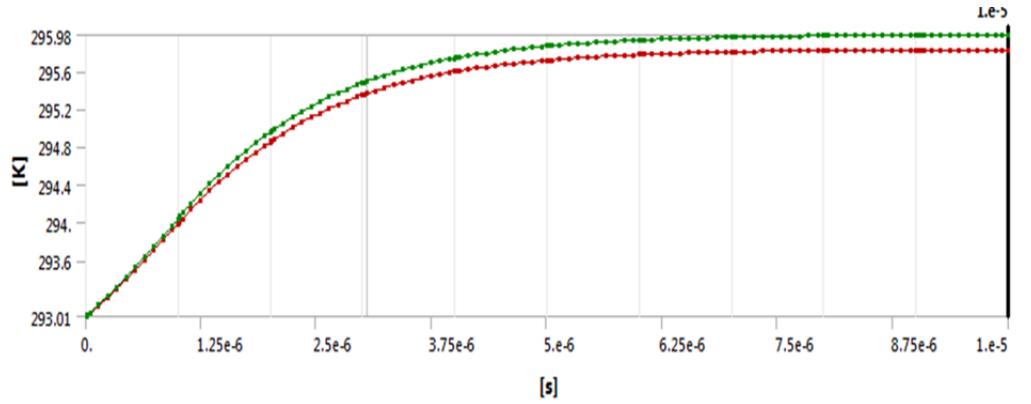


Figure 52: Teflon face pulse response from COMSOL.

The pulse-response of the Teflon face behaves as expected. The concavity changed as the heat flux input decreased. This showed that COMSOL can simulate a fast thermal pulse response at a high heat flux level.

The cooling phase of the pulse was also explored. The same heat flux model was used as in the previous test, with the exception of a 1 second “train” of 0 heat flux that was added onto the end of the pulse, simulating a 1Hz firing frequency. The results of this test are displayed in Figure 53.

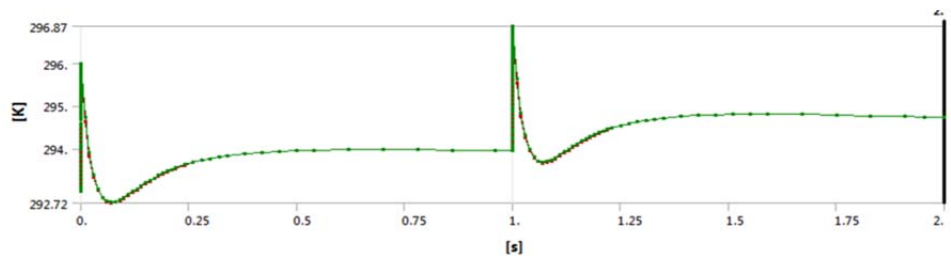


Figure 53: Pulse response with cooling from COMSOL.

The results in Figure 53 show an obvious error, as the temperature drops below the ambient temperature during the cooling phase. This is likely due to the heat flux being discontinuous after the pulse, and the time-steps are too large. In later pulse-response simulations these problems were addressed.

For simulating long time periods, the method of entering pulses as tabular data is extremely inefficient. With 11 time steps to simulate a pulse, simulating anything more than 10

pulses becomes very time intensive and error prone. Since the function capabilities of COMSOL were not known at this point in the process, the pulse method was abandoned.

For the long time period simulations, a method of a single long pulse was adopted. This involved applying a single high-magnitude heat flux for several hundred pulsing periods to simulate an extreme worst case scenario. In testing this method a heat flux within the same magnitude of those previously used was chosen, and due to time constraints the flux was applied to a 2-D model. While the Teflon face showed the proper response, the second set of elements showed sub-ambient temperature as in Figure 54.

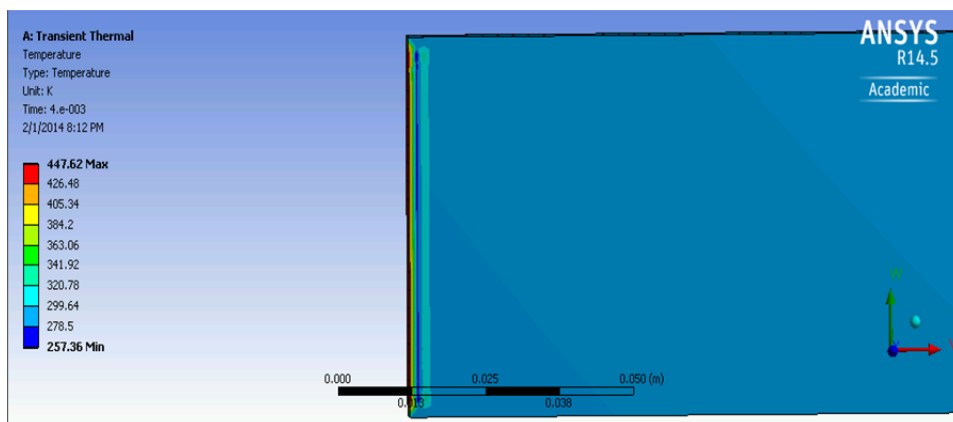


Figure 54: 2-D long pulse error in ANSYS.

This same simulation was also run in COMSOL with a lower heat flux to compare with ANSYS, as shown in Figure 55.

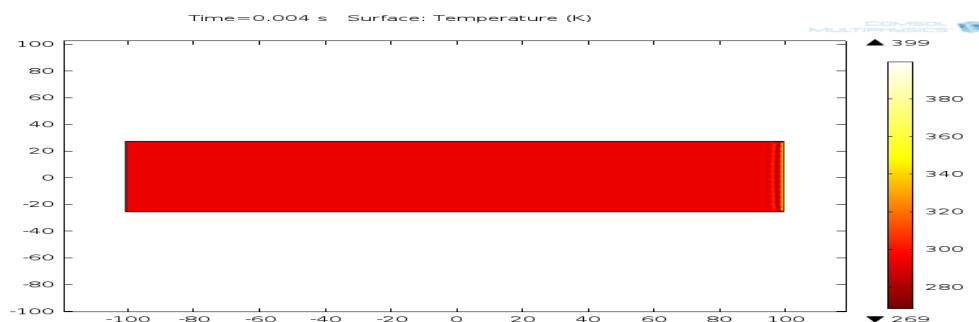


Figure 55: 2-D long pulse error in COMSOL.

Upon further investigation it was determined that the magnitude of the sub-ambient error was dependent on the magnitude of the applied heat flux, increasing as the heat flux increased. Due to this behavior, as well as the fact that the heat flux is applied as a function with a jump discontinuity, it is likely that this error is caused by the Gibbs phenomenon. This phenomenon

happens when a function with a jump discontinuity, such as a square wave, is approximated using a Fourier series (Cha and Molinder, 2006). It causes an overshoot and oscillations that are proportional to the magnitude of the discontinuity, in this case, the suddenly applied heat flux. In the end the long pulse method was not used both due to the errors in the models used, and that it would not give a realistic result anyway. It did however provide some information in how to proceed in latter iterations. When heat fluxes were to be applied in later studies, they would have to be “smoothed”, so as to avoid introducing the error causing jump discontinuity.

To create a more accurate solution, a pulsed profile that would simulate the realistic profile being applied to the thruster had to be created. This would require making a time dependent function that could be input to the model as the heat flux. Due to COMSOL’s better ability to implement such functions, it was used. The characteristics of this pulse were derived from the performance model shown in Table 3 (Laperriere et al., 2007) that provides the electric current flowing through the micro-PPT circuit and a pulse duration of about 0.6E-6s.

An input pulsed function into COMSOL was derived. To simulate a single pulse, a rectangular function was used. This function required a lower bound, the beginning of the pulse, and an upper bound, the end of the pulse. In order to avoid the problems with jump discontinuities encountered earlier a smoothing factor was also introduced. This used to derivatives to create a 0.05E-6s section before and after the pulse that would gradually ramp up to the full value of 1. The parameters of the rectangular function are given in Table 15 and the function is plotted in Figure 56.

Table 15: Parameters of sample rectangular thermal input function to COMSOL.

Lower Bound	0.05E-6 s
Upper Bound	0.65E-6 s
Smoothing Derivatives	2
Smoothing Length	0.1E-6 s

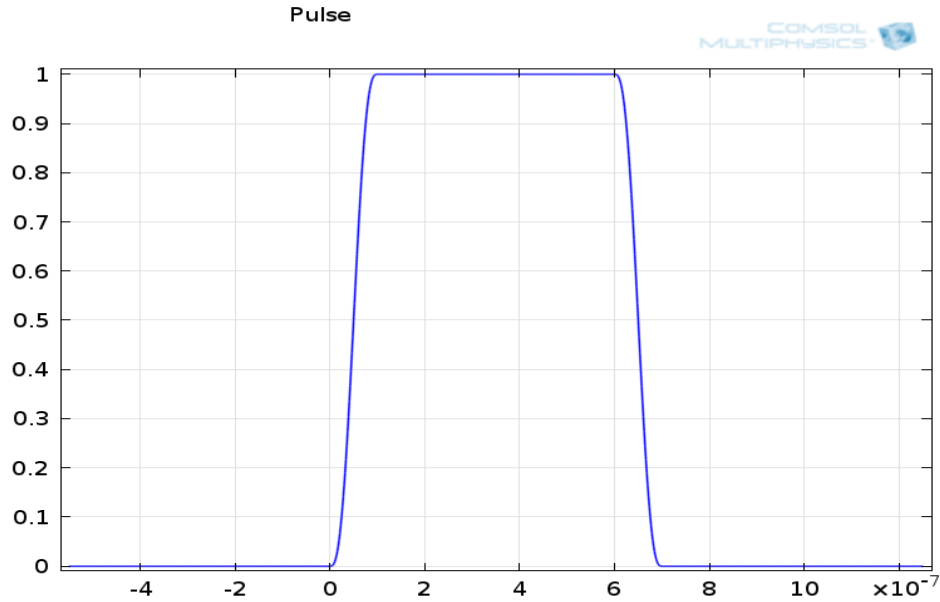


Figure 56: Rectangular pulse input function.

A function was also generated to apply the pulse at a 1Hz firing rate. This was accomplished using the modulo operator mod (main function argument, period). This operator was given arguments of $t[1/s]$ (expects unit-less first argument) and 1, the 1s period. The function created had an expression of

$$Pulse_{Function} = Pulse\left(\text{mod}\left(t\left[\frac{1}{s}\right], 1\right)\right) \quad (4.3)$$

with an argument of t . The plots of this function are given in Figures 57 and 58.

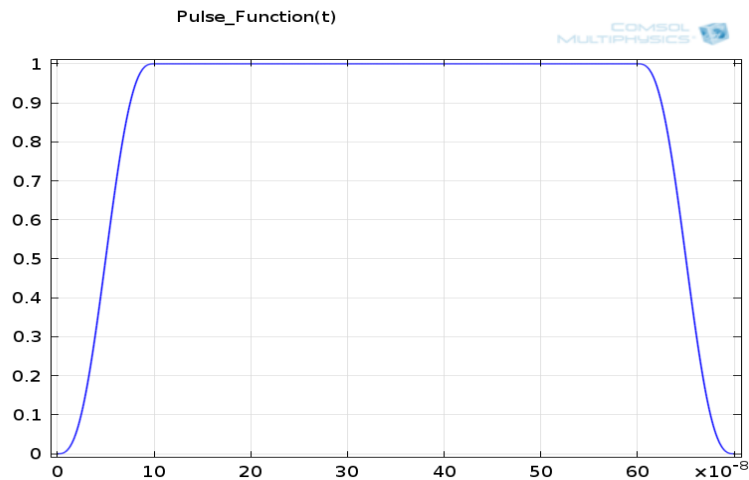


Figure 57: Up-close pulse modulation function.

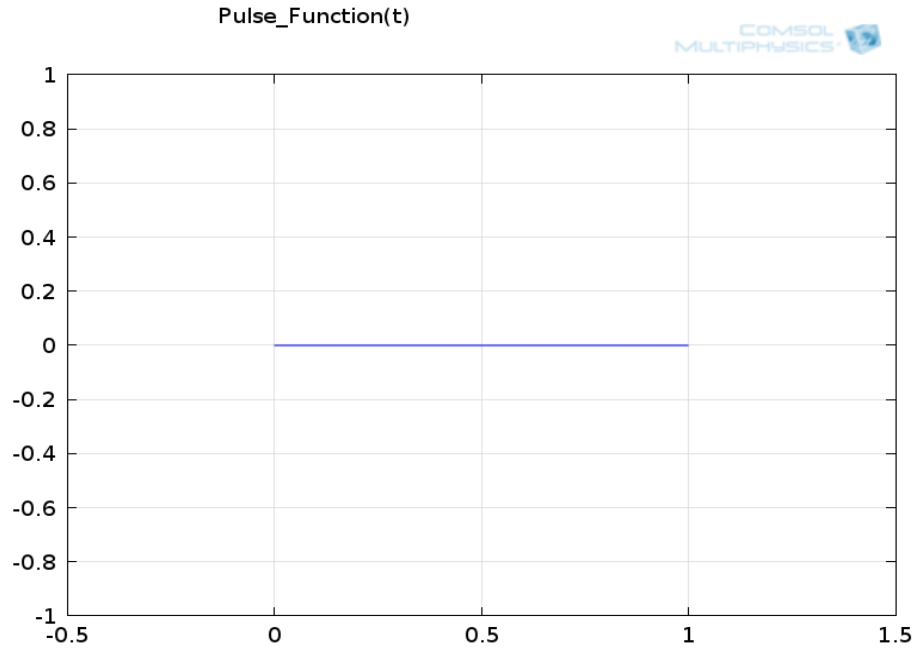


Figure 58: 1 period modulation function.

Note that Figure 58 does not show a pulse due to plot resolution. Figure 59 shows the modulated function with an elongated pulse length.

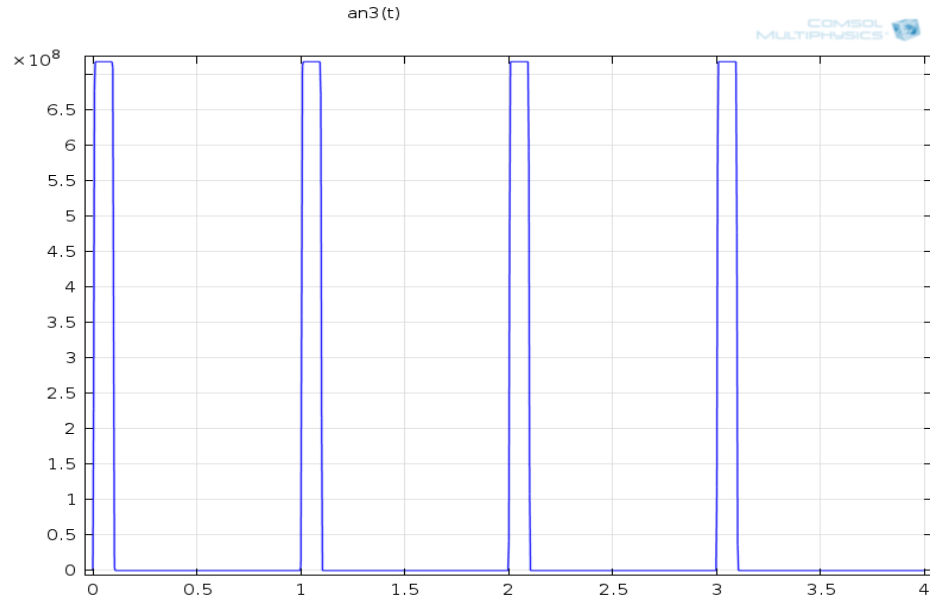


Figure 59: Elongated pulse length.

To implement the pulsed heat flux involved merely multiplying the previous function (which was binary, outputting 1s or 0s) by the desired heat flux magnitude:

$$Heat_Flux(t) = (\dot{q}) * Pulse_Function(t) \quad (4.4)$$

The result is shown in Figure 60.

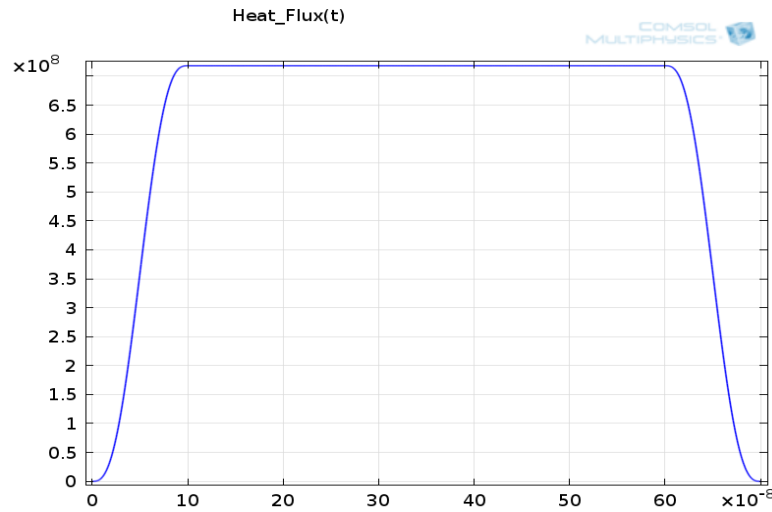


Figure 60: Up-close pulse of heat flux function.

4.3 Pulsed Model Validation

The first validation was based using Scenario 1 presented in in Figure 48. This validation used the characteristics in Table 3, heat flux of $7.18E8 \text{ W/m}^2$, frequency of 1Hz, and a $2 \mu\text{s}$ duration applied heat flux. A problem occurred in trying to recreate the same 600-12000 pulses used in Case 2. Due to the great difference between the length of the pulse and the length of the train in the pulse function there were significant issues with the simulation's time stepping in COMSOL. If a long time step was used, one that could solve the train in a reasonable amount of time, but the heat flux pulse would often be missed. Use of short time step, one with the resolution to accurately model the effect of the heat flux pulse, the train would take an unreasonably long period to solve. Two approaches were considered to address the issue of variable time stepping. One was to use COMSOL's MATLAB integration to create a function that would vary COMSOL's time stepping automatically based on the phase of the solution. This would provide control over the time steps used but due to the programming skill and time required this method was not adopted in this MQP.

Instead a simpler method would be used. This involved solving the model over different solution periods. For each firing, the model would first be solved over the length of the pulse using a small time-step. Following this solution the model would be applied over the length of the train using a longer time-step. COMSOL automatically takes the solution of the previous

solution period as its initial condition, and so long as the previous solution solved up to the start of the next solution, this can be done without need of interpolation.

This approach required two arguments, comprised of three sub arguments per firing. Simulation of more than 20 firings became very laborious and error prone. Therefore the validation and all following simulations were run for 20 firing periods. Using the variable time stepping method the validation Case 2 was run for 20 firing periods. Figure 61 shows the results of the COMSOL simulation, with the temperature at 5, 10, 15, and 20s displayed vs. the position in the domain.

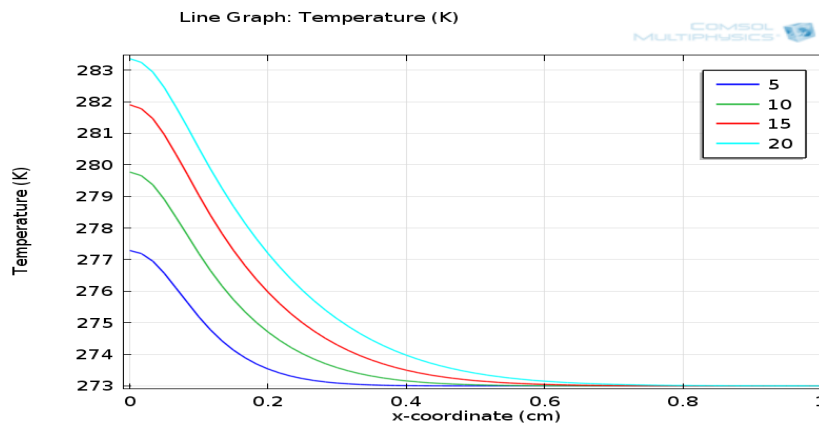


Figure 61: Pulsed thermal model COMSOL simulation of Case 2.

Figures 62 and 63 show the computational domain after a pulse and after a train respectively. Note that the face cools as the heat dissipates during the off-period as expected.

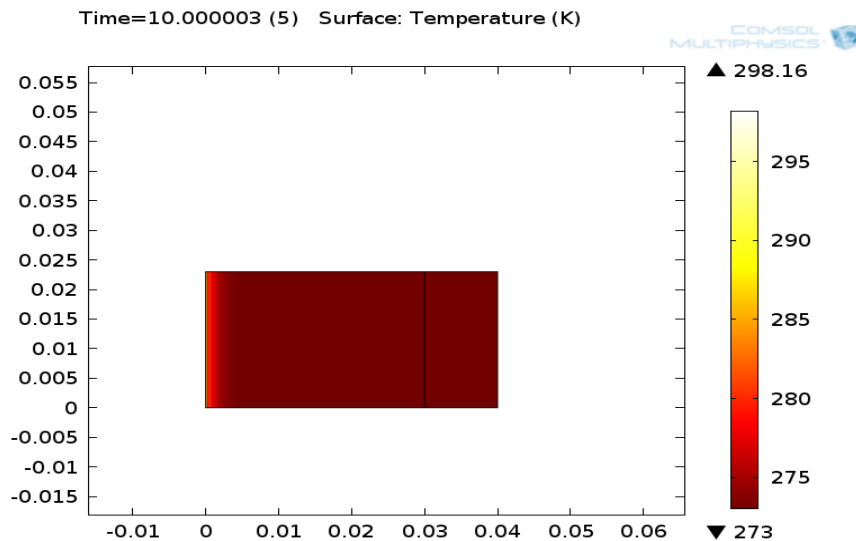


Figure 62: COMSOL simulation of Case 2 at 10sec +1 pulse.

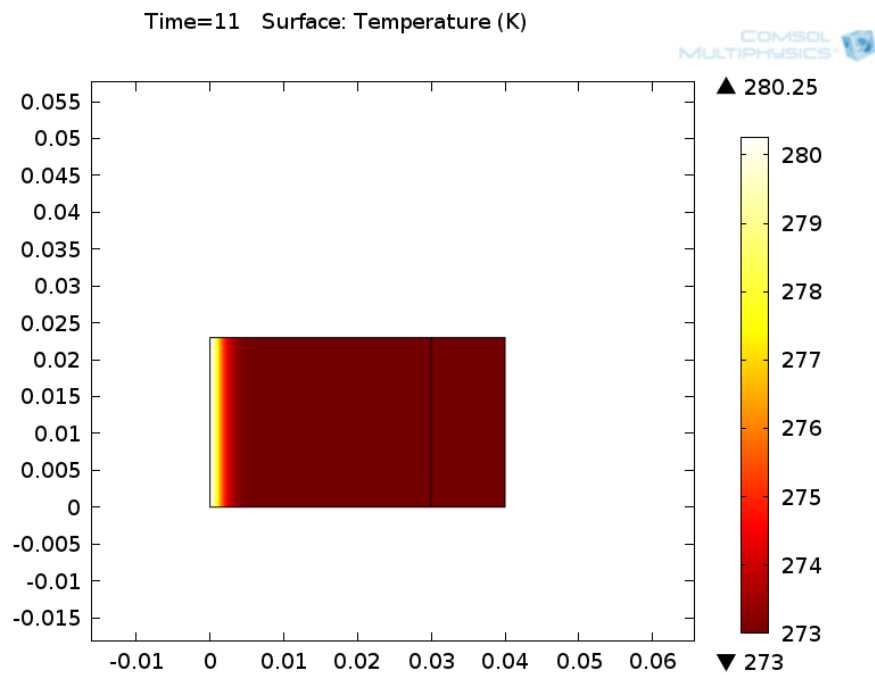


Figure 63: Simulation for Case 2 at 11sec.

Due to the fact that the COMSOL validation could only be run for 20 pulses, the results could not be compared directly with those of Case 2. However, since the results show general agreement with Figure 48, we concluded that the pulsing function worked well enough for process to continue.

The entire micro-PPT model shown in Figure 64 simulated using the pulsed heat flux.

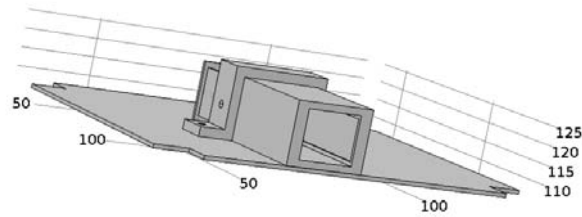


Figure 64: Micro-PPT Geometry in COMSOL.

This model, created in SolidWorks, was imported into COMSOL for analysis. The materials used in the model are given in Table 16.

Table 16: Material used in COMSOL thermal analysis of micro-PPT.

Electrodes	Copper
Casing	Torlon
Propellant	Teflon
Bracket	Structural Steel
Plate	Structural Steel

Note that despite the fact that tungsten-coated copper was chosen for the electrode material, copper was used in the model due to the fact that the thickness of the tungsten was unknown. Given its low thickness, it was assumed that the tungsten layer will have a minimal impact on the conductive behavior of the electrodes. The model was then meshed, with the results displayed in Figure 65.

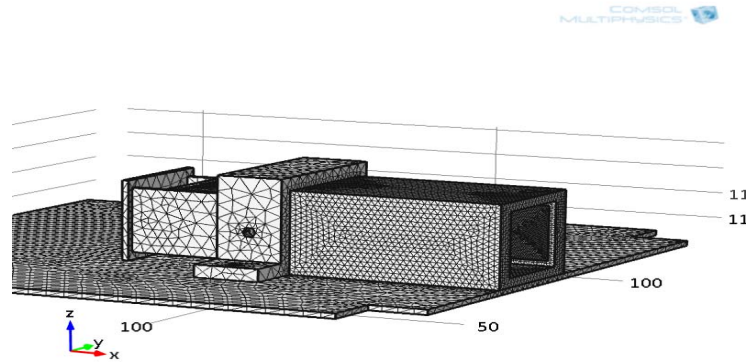


Figure 65: Micro-PPT meshed in COMSOL.

A variable mesh was used, with more fine elements being used in the domains in contact with the imposed heat flux where the thermal gradient would be highest, and larger elements being used in the domains not in direct contact with the heat flux.

However, before any simulation in relation to the micro-PPT design was to be conducted a validation of the full micro-PPT model was done. This validation used the heat fluxes from Case 2, with the heat flux being scaled based on the ratio of the discharge chamber heat flux to the Teflon area flux. The pulse width and frequency were also kept the same. The key parameters of this simulation are listed in Table 17.

Table 17: Parameters of full micro-PPT thermal simulation in COMSOL.

Initial Temperature	293 K
Teflon Heat Flux	7.18E8 W/m ²
Chamber Heat Flux	8.27E8 W/m ²
Pulse Width	2 μs
Firing Frequency	1 Hz
Lower Bound (Rect. Function)	0.25E-6 s
Upper Bound (Rect. Function)	2.25E-6 s
Smoother Transition Zone	0.5E-6 s

This simulation was run for 20 firings. Using COMSOL's built-in ability to calculate weighted averages, the change in the average surface temperature of the Teflon, electrode, and casing faces were plotted against time in Figures 66, 67, 68 respectively.

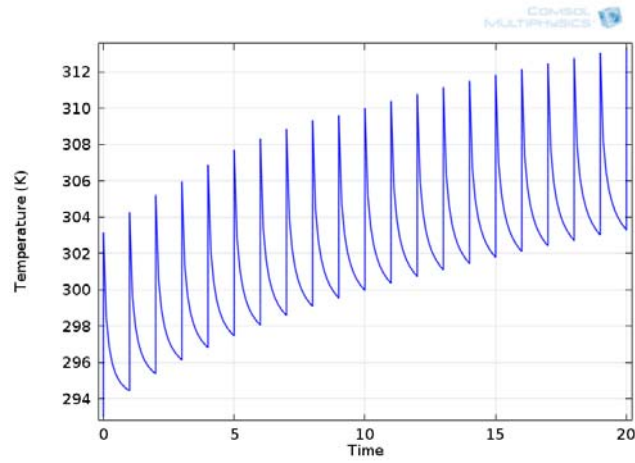


Figure 66: Average value of Teflon face temperature for high thermal flux.

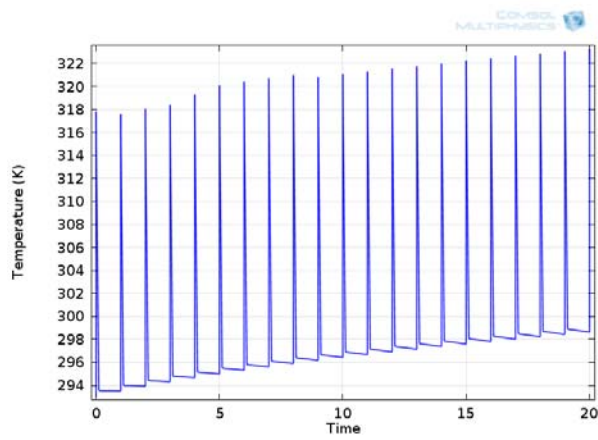


Figure 67: Average value of electrode face temperature for high thermal flux.

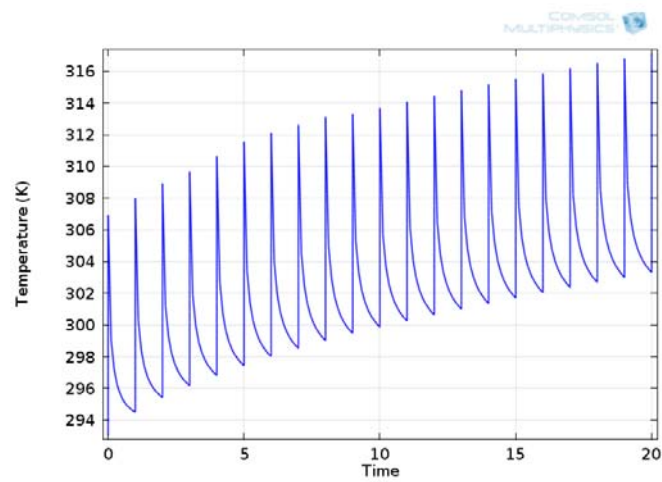


Figure 68: Average value of casing face temperature for high thermal flux.

The results of the simulation in Figures 66, 67, 68 show that the response of the micro-PPT model to the pulsed heat flux is as expected. The temperature rapidly increases over the pulse and decays over the duration of the train. Furthermore, the decay period depends on the thermal conductivity of the material, with the electrodes cooling faster, as expected. In order to compare the magnitude of the results to a verified model, the more simple Teflon domain simulation had to be run again, this time with initial temperature of 293 K, as in the above simulation. The average face (line) temperature versus time of this simulation is displayed in Figure 69.

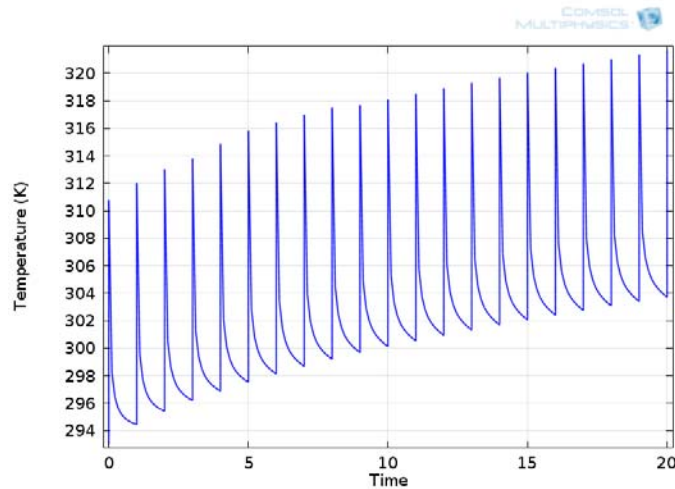


Figure 69: Teflon domain average face temperature with high thermal flux.

4.4 Thermal Performance of the micro-PPT Design

COMSOL was used to simulate the thermal performance of the micro-PPT considered in this MQP shown in Table 3. The total discharge energy is 0.2432 J with a pulse period of 0.6 μ s period. By dividing the discharge energy by this pulse time, the input power was found and assuming a percentage of the discharge energy lost to the PPT chamber as heat from Bushman and Burton, (2001), the thermal input power was found for the Teflon and discharge chamber domains. Finally, by dividing the thermal input powers by their respective areas of effect, the heat flux into the Teflon and chamber faces can be found. The final parameters input to the model are shown in Table 18.

Table 18: Parameters used in thermal analysis of the micro-PPT.

Discharge Energy	0.2432 J
Pulse Length	0.6 μ s
Pulse Input Power	405.333 kW
Teflon Thermal Power (@ 5% of Discharge)	20.3 kW
Chamber Thermal Power (@ 70% of Discharge)	283.8 kW
Exposed Teflon Face Area	147 mm ²
Exposed Chamber Face Area	1789 mm ²
Teflon Face Heat Flux	1.38E8 W/m ²
Chamber Face Heat Flux	1.59E8 W/m ²
Lower Bound (Rect. Function)	0.05 E-6 s
Upper Bound (Rect. Function)	0.7 E-6
Smoothing Transition Zone	0.1 E-6 s
Firing Frequency	1 Hz
Initial Temperature	293 K

This simulation was run for 21 firings. Figure 70 shows the thermal distribution through the micro-PPT after a pulse, and Figure 71 shows the distribution after a train. The micro-PPT conducts and cools as expected. It should be noted that the distribution still shows slightly below ambient temperatures. This is still likely due to the Gibb's Phenomenon encountered earlier, and could be reduced by a longer smoothing period.

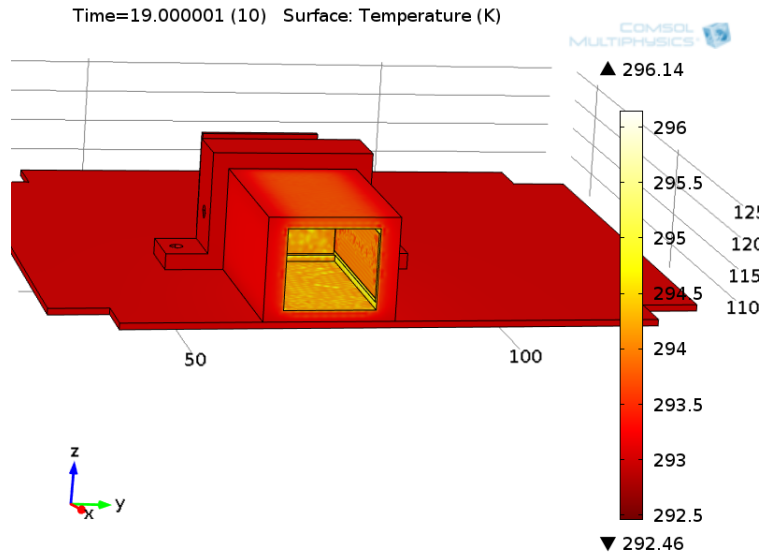


Figure 70: Temperature distribution in a micro-PPT after a pulse.

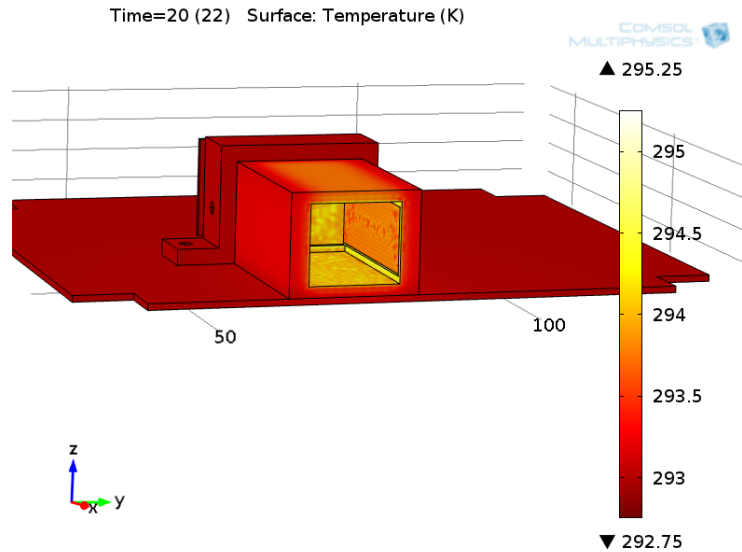


Figure 71: Temperature distribution micro-PPT after a train.

To better determine the micro-PPT's response to the pulsed heat flux, area averaged face values were once again taken. The averaged values of the Teflon, electrode, and casing faces are shown in Figures 72, 73, and 74 respectively. As in the validation case, the temperatures show the same pattern of rapid increase during the pulse, decay during the train, and a gradual temperature rise with time.

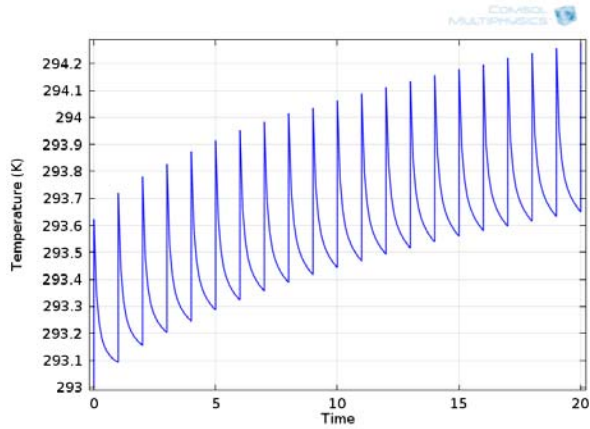


Figure 72: Average Teflon face temperature in the micro-PPT.

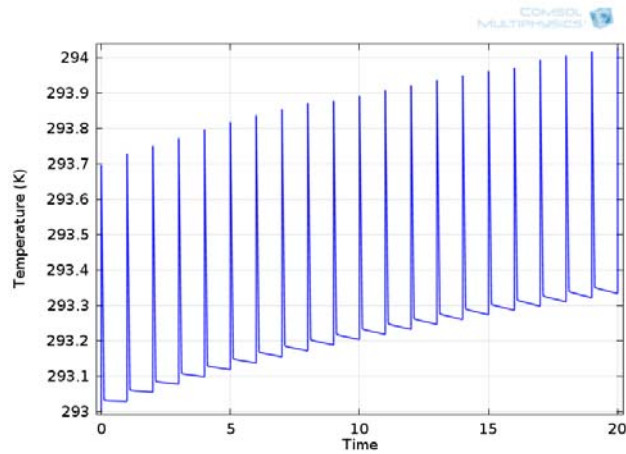


Figure 73: Average electrode face temperature in the micro-PPT.

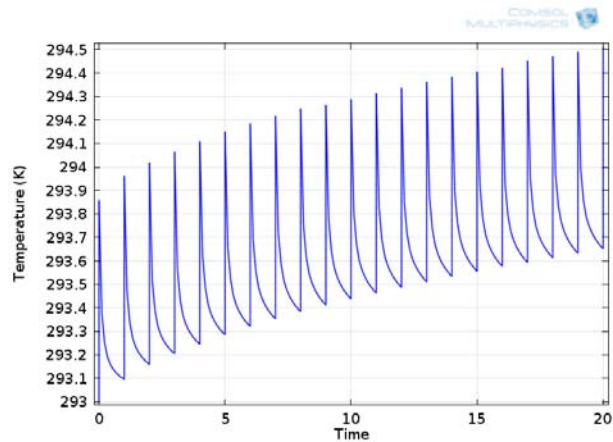


Figure 74: Average casing face temperature in the micro-PPT.

In order to determine the long term thermal performance of the micro-PPT, the maximum face values over time were taken. Since the maximum at the heated face of a domain represents

the global maximum, the maximum face values would allow the assessment of whether the micro-PPT could fail thermally over long pulsing period. Since the very leading edge of the Teflon would be expected to ablate, this maximum was not taken. Figures 75 and 76 show the maximum temperatures of the electrode and casing faces over time.

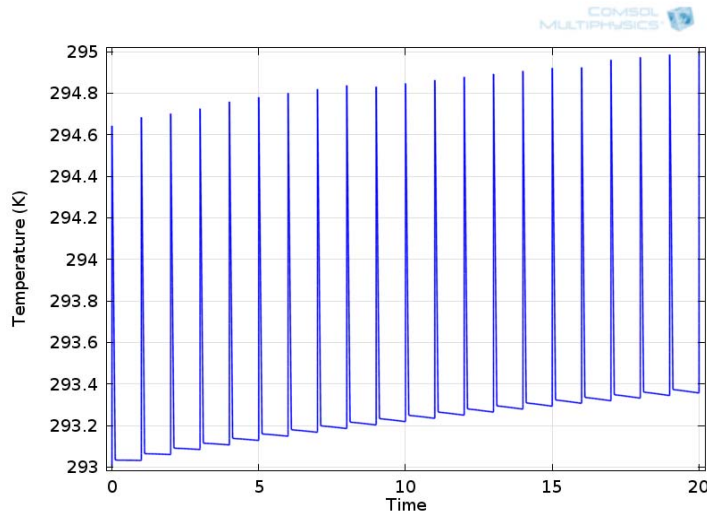


Figure 75: Maximum electrode temperature in the micro-PPT.

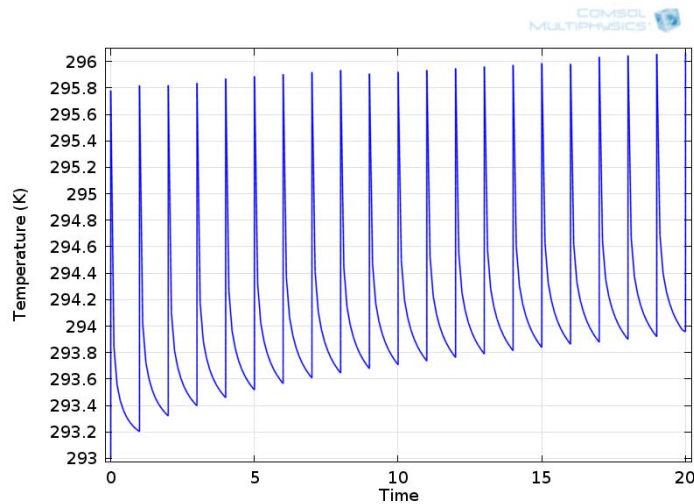


Figure 76: Maximum casing temperature in the micro-PPT.

Using these results a worst case maximum temperature for the electrodes and casing could be formulated. This arose from the realization that the time rate of increase in temperature, $\frac{\partial T}{\partial t}$, would decrease with time. Since the domain temperatures will increase, their radiative heat transfer to the largely thermally static ambient medium will increase. This, coupled with

unchanging input heat flux magnitudes, will lead to a lower dQ_{left} in the domain in time dt . Ultimately this will result in a decreasing $\frac{\partial T}{\partial t}$ over time, a negative $\frac{\partial^2 T}{\partial t^2}$. This is proven in Figures 77-80:

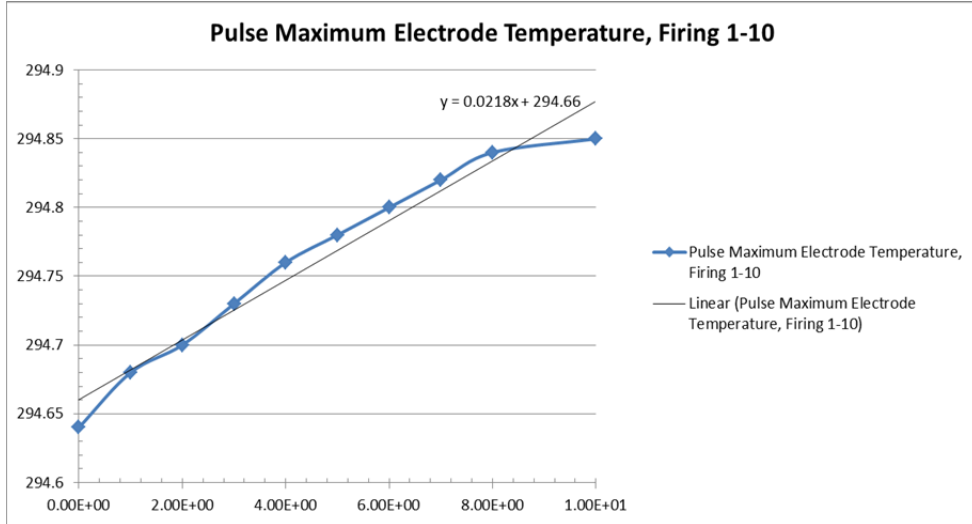


Figure 77: Pulse maximum electrode temperature, firing 1-10.

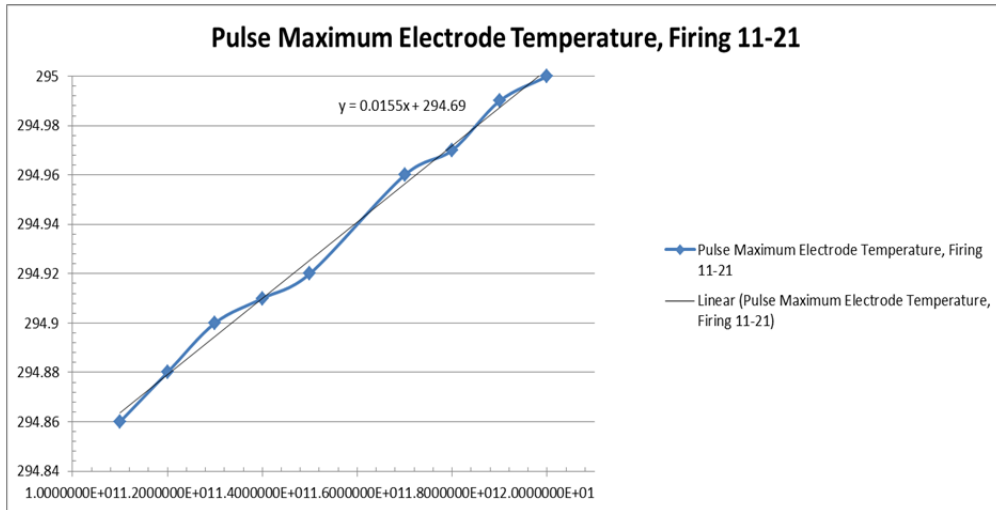


Figure 78: Pulse maximum electrode temperature, firing 11-21.

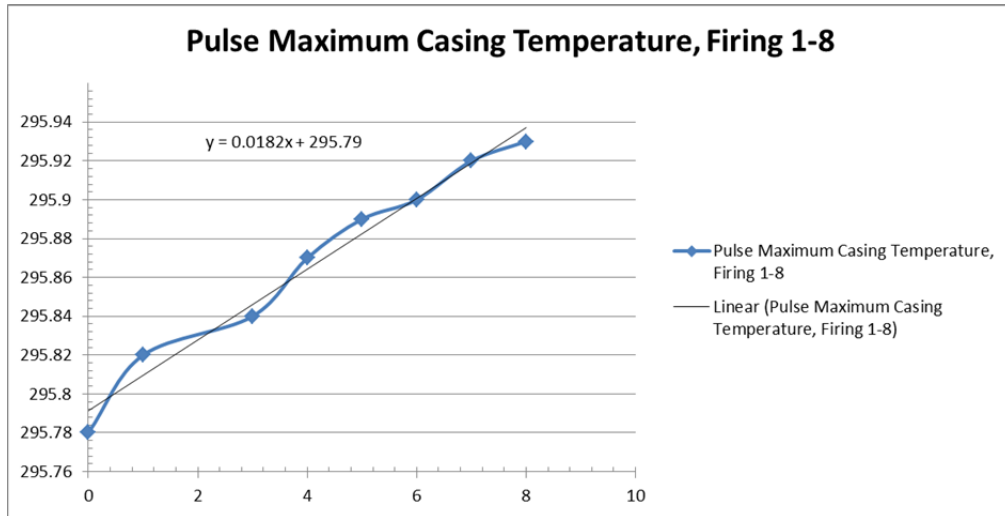


Figure 79: Pulse maximum casing temperature, firing 1-8.

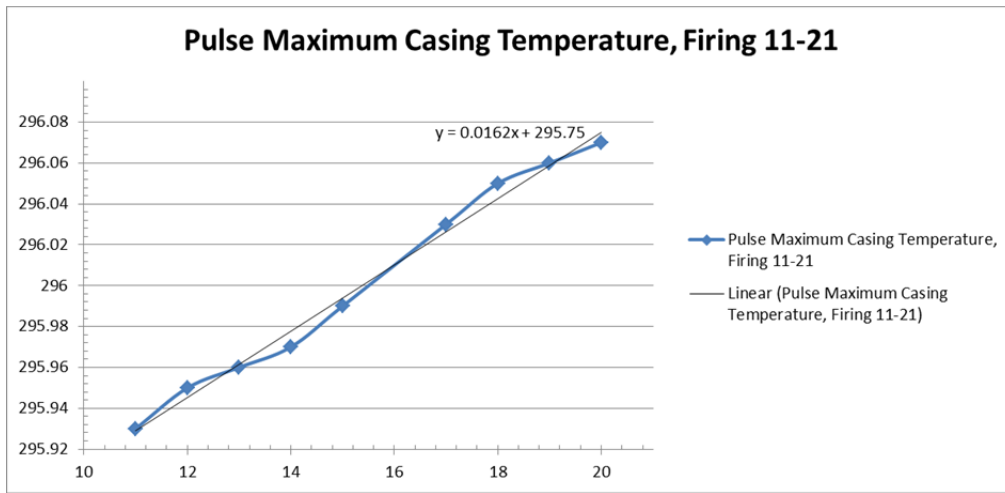


Figure 80: Pulse maximum casing temperature, firing 11-21.

The data used in Figures 77-80 was taken from the maximum surface temperature over time tables derived in COMSOL. The specific data points used were the points just after the pulse periods, where the temperature was maximum for the firing period. These data points represented the ΔT values to be used in determining the worst case $\frac{\partial T}{\partial t}$. Note that some data points are missing from Figures 77-80. These data points corresponded to outlier temperatures, and were accordingly removed. The slopes taken to the data points in Figures 77-80 clearly show that the slopes during the earlier firing periods are greater than those of the later firing periods. Therefore $\frac{\partial T}{\partial t}$ is clearly shown to decrease over time.

Since $\frac{\partial T}{\partial t}$ will decrease over time, $\frac{\partial T}{\partial t}$ over the early solution period will be a worst case when used to evaluate longer solution periods. Therefore the data from Figures 75 and 76 can be used to find the worst case approximate maximum temperatures on the electrode and casing domains at an arbitrary firing time using the following equation:

$$T_{max}(t) = \frac{\Delta T_{Firing\ 1-21}}{\Delta t_{Firing\ 1-21}} \Delta t_{Firing} + T_{Firing\ 1} \quad (4.3)$$

The $\frac{\Delta T_{Firing\ 1-21}}{\Delta t_{Firing\ 1-21}}$ values, evaluated using the maximum temperature data after the pulse periods from COMSOL are given in Table 19.

Table 19: $\frac{\Delta T_{Firing\ 1-21}}{\Delta t_{Firing\ 1-21}}$ values.

Electrode	Firing 1 Time	7E-6 s
	Firing 21 Time	20.000007 s
	Firing 1 Temperature	294.64 K
	Firing 21 Temperature	294.998 K
	$\frac{\Delta T_{Firing\ 1-21}}{\Delta t_{Firing\ 1-21}}$	0.0174 K/s
Casing	Firing 1 Time	7E-6 s
	Firing 21 Time	20.000007 s
	Firing 1 Temperature	295.781 K
	Firing 21 Temperature	296.067 K
	$\frac{\Delta T_{Firing\ 1-21}}{\Delta t_{Firing\ 1-21}}$	0.0143 K/s

A solution time of 20000s, 1000 times greater than the current solution time, was chosen. Evaluating Eq. (4.3) using the $\frac{\Delta T_{Firing\ 1-21}}{\Delta t_{Firing\ 1-21}}$ values of Table 21 and an approximate Δt_{Firing} time of 20000s, the results of Table 20 are found.

Table 20: Worst Case Approximation Electrode and Casing Temperatures at 20000s.

Worst Case Electrode Temperature at 20000s	642.64 K
Worst Case Casing Temperature at 20000s	581.781 K

The melting points of the PPT materials from CES EduPack (Granta, 2013) are given in Table 21.

Table 21: Melting points of micro-PPT materials.

Torlon	643 K
Copper	1350 K
Tungsten	3680 K

When the values of Tables 22 and 23 are compared, it can be seen that worst case approximation temperatures of the materials are less than their respective melting points. This leads to the conclusion that the PPT design should not fail thermally under long-term pulsing.

5.0 Conclusions and Recommendations

Pulsed Plasma Thrusters are good options for a Cubesat's propulsion subsystem due to their low power input, high specific impulse, and ease of geometric scalability. A micro-PPT is an even more attractive option because of its small size which makes integration into a 3U Cubesat possible. Although PPTs are limited by their low efficiencies they prove to be structurally integrateable with 3U Cubesat architecture. This MQP provides the conceptual design of a micro-PPT with focus on structural, electrical, and thermal considerations to meet the propulsion subsystem requirements of a 3U Cubesat. A PPT performance model (Laperierre et al. 2005,) and a PPT ablation model (Gatsonis et al, 2005; Stechmann 2007) was used to obtain the basic geometrical and performance characteristics of the micro-PPT. SolidWorks was used for design, ANSYS for structural analysis, and SPICE for electrical design, simulations, and COMSOL for thermal design and analysis.

5.1 Conclusions

5.1.1 Mechanical Design and Structural Analysis

The mechanical design of the micro-PPT required structural integrity in order to pass vibrational tests and maintain the highest performance characteristics realistically attainable. The iterative design process was based on SolidWorks to generate 3D models. Performance characteristics and geometrical features of the micro-PPT were provided by the performance and ablation models (Stechmann 2007). The expected operational environments proved a challenge and the design's parts were given specific shapes so that during take-off and orbit they would not slide out. The final model had a simple design held together by the compressive force of the back spring as shown in Figure 81.

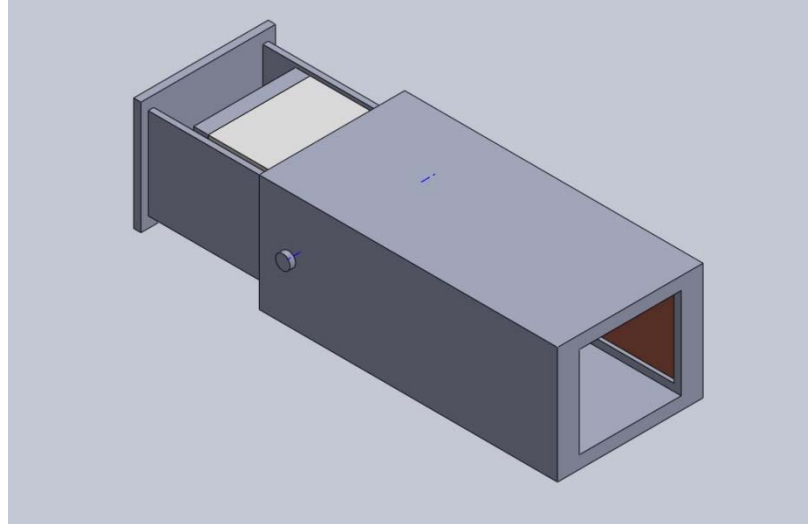


Figure 81: Final Model.

Material selection was performed to create a micro-PPT that could handle all necessary loads and requirements. Torlon 4203 was used as a housing material. Tungsten plated copper was selected to be used for the electrodes to resist spattering. Applying these materials to the SolidWorks model vibrational testing was conducted. Various simulations were performed using ANSYS to assure the structural integrity from the vibrational loads that may be expected. These loads were based on the worst case scenario presented by the NASA GEVS spaceflight verification document. The stresses and directional deformation as a result of the loads was negligible and therefore the design can be proceed for space qualification. The goal of the propulsion assembly is to allow 3-axis yaw, pitch a roll control of a 3U Cubesat. Therefore, integration of 8 Micro-PPTs into the 1U Cubesat was performed and modeled with an emphasis on structural redundancy for proper distribution of the center of mass which can be seen in Figure 82.

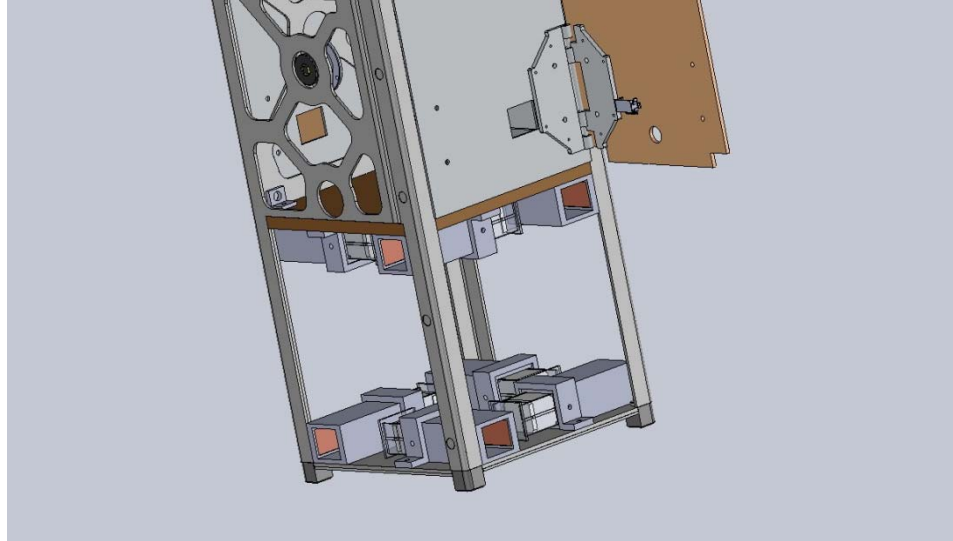


Figure 82: 3-axis control configuration

5.1.2 Electrical Design and Analysis

The micro-PPT designed in this MQP is powered by Clyde Space's PPU. The PPU has limited capabilities and needs the addition of a PDM for proper switching and availability of enough connections for the 8 Micro-PPTs. The PDM provides anywhere from 1W – 19W of instantaneous power. The voltage levels at the input of our Vacuum Arc Ignition system are 3.3V and 5V.

The Vacuum Arc Ignition system designed in this MQP needs to be able to generate two different high voltage, 750V and 1500V pulses. The 1500V pulse is required for an initial discharge to ablate a piece of Teflon[®] and ionize it. The 750V pulse is to begin conduction through the plasma to generate the current sheet that gets accelerated by the Lorenz Force.

The circuit topologies for main and initial discharge were designed. The circuit topology for the main discharge consisted of a main capacitor that gets charged by a proportion high voltage DC-DC converter. The PDM switches at the right appropriate frequency to control the charging and discharging cycles.

The circuit topology for the initial discharge consists of two capacitors that get charged by a high voltage DC-DC converter. These two capacitors will be connected in a Marx-Bank Circuit configuration. Essentially, they charged in parallel to the high voltage DC-DC converter potential, and then discharged in series to double the voltage provided by the DC-DC converter.

Circuit simulations using P-SPICE were generated to confirm the functionality of both circuit topologies. Afterwards, the design was drawn on ULTIBOARD for a structural overview

of the dimensions the PCB board would take up. It was determined the PCB board would be adequate in size to fit in the bottom third of the 3U Cubesat. The PCB board was designed for minimal EMI and redundancy was used for balance of the center of mass of the board.

5.1.3 Thermal Design and Analysis Model

The thermal modeling has yielded several results. First it was determined that Finite Element Analysis was the best way to conduct the analysis on the complex heat transfer problem provided. Second it was verified that FEA offers an accurate means of simulating transient heat conduction. Third it was discovered that COMSOL offers the best solution to simulating a PPT, due to its ability to easily create pulsed input functions. Fourth it was verified that the pulsed model implemented in COMSOL exhibited the correct and expected behavior. Finally the thermal behavior of the PPT model was determined using the pulsed PPT model in COMSOL and a worst case approximation was derived from this to determine that PPT design should not fail under the expected thermal loads during long-term pulsing

5.2 Recommendations for Future Work

The recommendations for the micro-PPT electric design are:

- Avoid using high voltage circuit if possible to avoid electrical arcing
- Try to use high current circuits instead because this will avoid electrical arcing and will create a higher Lorentz Force
- Make sure all electrical components purchased are hermetically sealed so that they can operate accordingly in space environments
- Include EMI models for PCB topologies to assure components are not interfering with one another. Current will always flow through the path of least resistance and sometimes this may be through a different path than expected.
- Have a systematic approach for identifying the best ground reference to use. If the same ground reference is not used for all components your components may electrically float creating noisy signals that require more filtering.

The recommendations for thermal design concern the improvement of the pulsed COMSOL model and the expansion of the scenarios modeled. To improve the COMSOL model future teams should consider:

- Using a MATLAB based solution for changing COMSOL's solver time-step based on whether the pulse or train is being solved. If this method can be implemented it will allow the model to be solved more easily and efficiently for longer firing periods.

- Should consider updating boundary conditions. Investigate different thermal loss efficiency values to improve the accuracy of applied heat flux values. Consider adding surface-to-surface radiation between applicable boundaries. If possible, experimentally validate model.

Future work should also consider:

- Using the improved COMSOL model to simulate for firing periods in excess of 1000, with a goal of 20000. This will allow better evaluation of PPT thermal performance under long duration firing.
- Expand the computational domain to include the 3U Cubesat. This will ensure that thermal losses through the micro-PPT do not negatively affect other Cubesat components.

Bibliography

- Annaratone, Donatello. *Engineering Heat Transfer*. Berlin: Springer-Verlag, 2010.
- Bushman, Stewart S., and Rodney L. Burton. "Heating and Plasma Properties in a Coaxial Gasdynamic Pulsed Plasma Thruster." *Journal of Propulsion and Power*, 2001.
- Cha, Philip D., and John I. Molinder. *Fundamentals of Signals and Systems*. Cambridge: Cambridge University Press, 2006.
- "Granta CES EduPack" Granta Material Intelligence. Granta Design Limited, 2013
- Gatsonis, N.A, Byrne. L., Zwahlen, J., Pencil, E., Kamhawi, H., "Current-Mode Triple and Quadruple Langmuir Probe Methods with Applications to Flowing Pulsed Plasmas," *IEEE Transactions on Plasma Science*, Vol. 32, No. 5, pp. 2118-2129, October 2004.
- Gatsonis, N.A., Eckman, R., Yin, X., Pencil, E.J., Myers, R.M., "Experimental Investigations and Numerical Modeling of Pulsed Plasma Thruster Plumes," *Journal of Spacecraft and Rockets*, Vol. 38, No. 3, pp. 454-464, May-June, 2001.
- Gatsonis, N.A., Juric, D. and Stechmann, D.P., "Numerical Analysis of Teflon Ablation in Solid Fuel Pulsed Plasma Thrusters," AIAA-2007-5227, 43rd AIAA/ASME/SAE/ASEE Joint Propulsion Conference, Cincinnati, OH, July 2007.
- Kumagai, Naoki, et al. "RESEARCH AND DEVELOPMENT STATUS OF LOW POWER PULSED PLASMA THRUSTER SYSTEM FOR μ -Lab Sat II." *28th International Electric Propulsion Conference*. Toulouse, France, 2003.
- Laperriere, D., Gatsonis, N.A. and Demetriou, M.A., "Electromechanical Modeling of Applied Field Micro Pulsed Plasma Thrusters," AIAA 2005-4077, 41th AIAA/ASME/SAE/ASEE Joint Propulsion Conference, Tucson, AZ, July 2005.
- Laperriere, D., "Electromechanical Modeling and Open-Loop Control of Parallel Plate Pulsed Plasma Microthrusters with Applied Magnetic Fields," Co-Advisor, M. Demetriou, M.S. Thesis, Worcester, MA, June 2005.
- Partridge, J., "Development and Implementation of Diagnostics for Unsteady Small-scale Plasma Plumes," Ph.D., Worcester, MA, September 2008.
- Partridge, J., and Gatsonis, N.A., "Characterization of High-Density Flowing Plasmas Using a Directional Micro-Retarding Potential Analyzer," IEPC-2005-170, 29th International Electric Propulsion Conference, Princeton, NJ, November 2005.

Pottinger, S. J., and C. A. Scharlemann. "Micro Pulsed Plasma Thruster Development." *International Electric Propulsion*. Florence: Electric Rocket Propulsion Society, 2007.

Encyclopædia Britannica Online [Internet]. Encyclopædia Britannica Inc.; 2014. [Cited 2014 March 5]. Available from: <http://www.britannica.com/EBchecked/topic/499323/resistivity>

Shaw, Peter Vallis. *Pulsed Plasma Thrusters for Small Satellites*. PhD Thesis, Surrey: University of Surrey, 2011.

David Stechmann, "Numerical Analysis of Transient Teflon Ablation" MS Thesis, Worcester, MA, July 2007

Munakata, Riki. *CubeSat Design Specifications Rev. 12. The CubeSat Program, Cal Poly SLO* Cal Poly, 2009

Crook, Mathew. *Cubesat Launcher Design, Process and Requirements*, Master's Thesis: NPS, 2012

Marques, R. Intini and Gabriel, S.B. *Design of a Two-Stage PPT for Cubesat Application*, University of Southampton, 2009

Strain, Andrew . *User Manual: 3U Electrical Power System CS-3UEPS2-NB Document No: USM-00007*. Clyde Space, 2011

NASA Goddard Space Flight Center. *General Environmental Verification Standard (GEVS) document number GSFC-STD-7000*.

All-State Industries *Torlon 4203 datasheet* accessed 12/15/13 <http://www.all-stateind.com/plastics/specshts/11/4203.pdf>

EMCO *datasheet* accessed 12/15/13 <http://www.emcohighvoltage.com/pdfs/qseries.pdf>

MULTISIM. Computer software. <Http://www.ni.com/>. Vers. 10. National Instruments

ULTIBOARD. Computer software. <Http://www.ni.com/>. Vers. 10. National Instruments

PSPICE. Computer software. <Http://www.cadence.com/>. Vers. 10. Cadence Design Systems

SolidWorks. Computer software. <Http://www.solidworkscom/>. Dassault Systemes SolidWorks Corp.

COMSOL Multiphysics. Computer software. <Http://www.comsol.com/>. Vers. 4.4. COMSOL